possibility of BRCA1-mediated RPB8 degradation. Therefore, we tested if BRCA1-BARD1 destabilized RPB8 *in vivo* under several different conditions, including BRCA1-BARD1 overexpression and BRCA1 knockdown by siRNA. FLAG-RPB8 was coexpressed in 293T cells with Myc-BRCA1$^{1-772}$ and HA-BARD1 (Fig. 3*A*). The steady-state level of FLAG-RPB8 increased upon coexpression of BRCA1-BARD1 in a dose-dependent manner in the soluble fraction (*lanes 1–4*) but not in whole-cell lysates (*lanes 5–8*). We then examined protein half-life of FLAG-RPB8 in the soluble fraction using cycloheximide, a protein synthesis inhibitor. The FLAG-RPB8 protein half-life was prolonged by BRCA1-BARD1 overexpression (Fig. 3*B*). We also tested the effect of BRCA1-BARD1 on endogenous RPB8 (Fig. 3*C* and *D*). The steady-state level of RPB8 only slightly increased upon coexpression of BRCA1-BARD1 in the soluble fraction (Fig. 3*C*, *lane 4*) and no effect was observed when whole-cell lysates were evaluated (*lanes 5–8*). However, RPB8 protein half-life was detectably shortened by BRCA1 knockdown (Fig. 3*D*). This observation was not detected when whole-cell lysates were analyzed (data not shown). Together, analyses of steady-state levels and protein half-lives indicated that only soluble RPB8 was stabilized, whereas that in whole-cell lysate was unchanged (Fig. 3). Alternatively, it was also possible that BRCA1-BARD1 shifted RPB8 from the insoluble fraction, such as the chromatin fraction, to the soluble fraction. However, we could not detect such a shift by fractionation analyses (data not shown). In either case, these findings at least suggest that BRCA1-BARD1–mediated RPB8 ubiquitination is not a signal for its degradation.

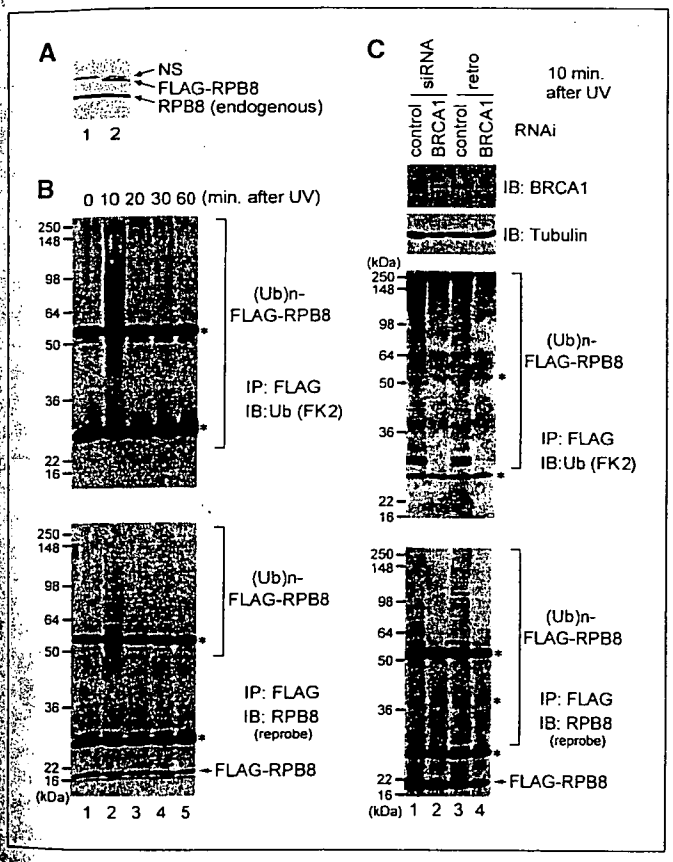

Figure 4. BRCA1-dependent RPB8 polyubiquitination in response to UV irradiation. *A*, parental HeLa cells (*lane 1*) and HeLa cells stably expressing FLAG-RPB8 (*lane 2*) were lysed with SDS-sample buffer and immunoblotted with anti-RPB8 antibody. *NS*, nonspecific products. *B*, HeLa cells stably expressing FLAG-RPB8 were UV irradiated (35 J/m^2) and harvested at the indicated times after irradiation. Ubiquitinated RPB8 was detected as described in Fig. 2*B*, except that anti-ubiquitin antibody (FK2) was used for immunoblotting (*top*). The membrane was reprobed with anti-RPB8 antibody (*bottom*). *C*, HeLa cells stably expressing FLAG-RPB8 were either transfected with control siRNA (*lane 1*), transfected with siRNA for BRCA1 (*lane 2*), infected with retrovirus expressing control shRNA (*lane 3*), or infected with retrovirus expressing shRNA for BRCA1 (*lane 4*). Cells were then UV irradiated (35 J/m^2) and harvested 10 min after irradiation. Cells were boiled in 1% SDS buffer and subjected either to immunoblotting with anti-BRCA1 (*top*) and antitubulin (*upper middle*) or to detection of RPB8 ubiquitination as in *B* (*lower middle* and *bottom*). *, IgG. Note that the different pattern of IgG detection between *B* and *C* is due to different lots of anti-FLAG cross-linked agarose beads.

BRCA1-dependent RPB8 ubiquitination after UV irradiation. BRCA1-mediated RPB8 ubiquitination prompted us to investigate the biological implications of this activity. We examined if RPB8 is ubiquitinated in response to DNA damage. Rather than exposing cells continuously to epirubicin, and because RPB1 is ubiquitinated after UV irradiation, we used UV irradiation to accurately determine the timing of RPB8 ubiquitination after DNA damage (22–25). We established HeLa cell lines that stably express FLAG-RPB8 at a low level (approximately one third of endogenous RPB8; Fig. 4*A*) to avoid artifacts caused by overexpression and analyzed ubiquitination of anti-FLAG immunoprecipitates with anti-ubiquitin (FK2) antibody. Because it has been reported that RPB1 ubiquitination occurs 1 to 2 h after UV irradiation (22–25), we first analyzed these time points. However, we did not detect any ubiquitination of FLAG-RPB8 (Fig. 4*B* and data not shown). Instead, ubiquitinated FLAG-RPB8 readily, and only transiently, appeared 10 min after UV irradiation (Fig. 4*B*, *top*). Reprobing the membrane with anti-RPB8 antibody verified that the detected ladder was ubiquitinated RPB8 (*bottom*).

To verify that UV irradiation–induced RPB8 ubiquitination requires endogenous BRCA1, RNA interference was used to knock down BRCA1 expression. HeLa cells stably expressing FLAG-RPB8 were transfected with BRCA1-specific siRNA. As a second alternative, we constructed a retrovirus engineered to express shRNA for BRCA1. Forty-eight hours after transfection or infection, cells were irradiated with UV (35 J/m^2) and then harvested 10 min later. Both the siRNA-transfected and the shRNA retrovirus–infected cells were successfully silenced for BRCA1 expression (>90% and >75% reduction, respectively) compared with their controls (Fig. 4*C*, *top*). As expected, RPB8 ubiquitination after UV irradiation was dramatically reduced by BRCA1 knockdown in both cases (*lower middle*). Reprobing the membrane with anti-RPB8 antibody again verified the ubiquitinated RPB8 that became completely undetectable upon BRCA1 knockdown (*bottom*). These results support the idea that RPB8 is polyubiquitinated by BRCA1-BARD1 in an early phase after UV irradiation.

A ubiquitin-resistant form of RPB8 retains its polymerase activity. For the purpose of studying the physiologic consequences induced by the BRCA1-mediated RPB8 ubiquitination after UV irradiation, we generated a mutant of RPB8 that is incapable of being ubiquitinated by BRCA1-BARD1. RPB8 possesses eight Lys residues in the whole protein (Fig. 5*A*). We first mutated single Lys residues of RPB8 and tested its capacity to be ubiquitinated. However, RPB8 ubiquitination was not dramatically reduced by each single mutation (Fig. 5*B*, *lanes 2* and *7*; data not shown). Instead, the ubiquitination of RPB8 was reduced as the number of Lys to Arg substitutions increased. This result recapitulates what we observed during studies of BRCA1 auto-ubiquitination and of BRCA1-mediated NPM1/B23 ubiquitination. When five of the eight Lys residues were substituted with Arg (5KR), RPB8 ubiquitination

became undetectable (Fig. 5*B*, *lane 5*), although its binding capacity to BRCA1-BARD1 was not reduced (data not shown).

To confirm that the many mutations required to make RPB8 resistant to ubiquitination did not impair its fundamental function as a subunit of RNA polymerases, we verified that the 5KR mutant is capable of binding to RPB1 or RPC155 (the largest subunit of polymerase III) *in vivo*. WT FLAG-RPB8 or 5KR was transfected into 293T cells, and anti-FLAG immunocomplexes were isolated. Bound proteins were resolved by SDS-PAGE and analyzed by immunoblotting using anti-RPB1 or anti-RPC155 antibodies. Both RPB1 and RPC155 were detected in the FLAG-5KR immunocomplexes as well as the WT immunocomplexes (Fig. 5*C*). We measured catalytic activity of the anti-FLAG immunoprecipitates using a runoff transcription assay. The 5KR mutant immunocomplexes contained the ability to generate *in vitro* transcripts equal to that of WT immunocomplexes (Fig. 5*D*). Thus, the 5KR mutation of RPB8 constitutes a viable RNA polymerase complex *in vivo* that sustains its polymerase activity. This indicates that RPB8 ubiquitination by BRCA1-BARD1 is not required for RNA polymerase activity.

Ubiquitin-resistant mutant of RPB8 causes UV hypersensitivity. BRCA1 deficiency causes hypersensitivity to DNA damage (14, 26, 27). Because RPB8 is ubiquitinated by BRCA1 after UV irradiation (Fig. 4), it was possible that failure to perform this function could cause the same phenotype. To test this possibility, we established HeLa cell lines that stably express the 5KR mutant of FLAG-RPB8. Two clones each of the WT (WT-1 and WT-2) and of the 5KR (5KR-1 and 5KR-2) cell lines were obtained (Fig. 6*A*). Polyubiquitination of FLAG-RPB8 after UV irradiation was detected in WT cells, but not in mutant cells (Fig. 6*B*). Using these cells, we examined if the expression of the mutant RPB8 affected cell survival after UV irradiation. The cell viabilities of the 5KR clones 48 h after 20 or 35 J/m^2 of UV irradiation were ~38% and 23% of untreated cells at 0 h, respectively, whereas WT clones were ~72% and 53%, respectively (Fig. 6*C*). Parental HeLa cells exhibited viabilities similar to that of WT clones (Fig. 6*C*). Representative data for cells observed by phase contrast microscopy 48 h after UV irradiation (35 J/m^2) and for culture plates stained with Lillie's crystal violet stain are shown (Supplementary Fig. S4). Thus, expression of a ubiquitin-resistant RPB8 form in cells causes UV hypersensitivity.

Because UV-induced cell death is largely ascribable to caspase-induced apoptosis, we next tested whether activation of the caspase pathway by UV irradiation was enhanced in 5KR cells. HeLa cell lines expressing WT or 5KR mutant of FLAG-RPB8 were UV irradiated, and caspase activity was measured by immunoblotting with an antibody to cleaved caspase-3. As shown in Fig. 6*D*, 5KR cells expressed larger amount of cleaved caspase-3 than WT cells did at each time point after UV irradiation. This result suggests that failure to ubiquitinate RPB8 after UV irradiation activates the caspase pathway, resulting in apoptotic cell death.

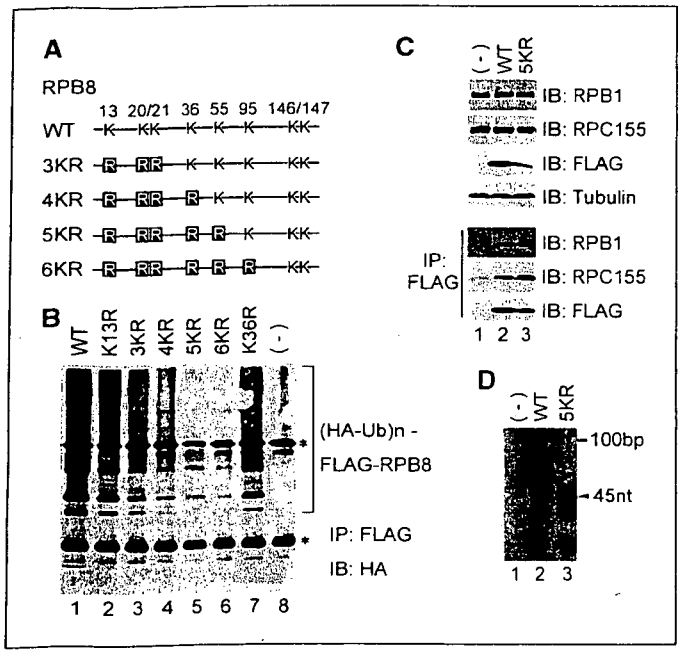

Figure 5. Construction of ubiquitin-resistant RPB8 mutant and assay of its RNA polymerase activity. *A*, the mutant constructs of RPB8. Lys (*K*) residues of RPB8 were substituted with Arg (*R*) as indicated. *B*, Myc-BRCA1$^{1-772}$, BARD1, and HA-ubiquitin were cotransfected into 293T cells either with WT or mutant FLAG-RPB8 as indicated. Polyubiquitination of RPB8 was detected as in Fig. 2*B*. *C*, 293T cells were transfected either with parental pcDNA3 vector (-), WT, or the 5KR mutant of FLAG-RPB8 as indicated. Total cell lysates (*top four panels*) or anti-FLAG immunoprecipitates from equal amounts of total cell lysates (*bottom three panels*) were subjected to immunoblotting with the indicated antibodies. *D*, anti-FLAG immunoprecipitates obtained as in *C* were subjected to an *in vitro* runoff transcription assay using double-stranded DNA templates designed to generate an RNA transcript of 45 nucleotides. Radiolabeled RNA products were resolved by a 12% polyacrylamide/urea gel and scanned with a Typhoon 9400 image analyzer. *, IgG.

Discussion

BRCA1 exists in several different supercomplexes to execute diverse cellular processes. In most of these complexes, BRCA1 exists as a RING heterodimer with BARD1 (28), the form that acquires significant ubiquitin ligase activity (6–8). Revealing the substrates specific for each BRCA1 protein complex is crucial to understand the mechanisms underlying its tumor-suppressor functions.

BRCA1-BARD1 complexes bind to BRCA2 and Rad51 and localize to discrete nuclear foci during S phase. After DNA damage, BRCA1 is phosphorylated by ATM/ATR family kinases (29, 30), and the BRCA1 foci disperse within 30 min (31). The BRCA2-Rad51–containing complex, as well as the BRCA1 complex with Mre11-Rad50-Nbs1, gradually reassemble into different foci (sites of DNA damage) and play important roles in homologous recombination repair. The BRCA1-containing foci begin to appear ~1 h after DNA damage has occurred, reach their peak after 6 to 8 h, and remain until 12 h after damage (31, 32). BRCA1-BARD1 also associates with the RNA polymerase II holoenzyme (15, 16). In contrast to the cases of other complexes described above, BRCA1 dissociates from hyperphosphorylated, processive polymerase II 1 h after DNA damage (17). However, how BRCA1 affects the polymerase II complexes, if at all, during the early stages after DNA damage and before the translocation of BRCA1 to the repair machinery remains to be elucidated. Our results suggest that BRCA1 polyubiquitinates a component of the polymerase II complex, RPB8, at this early stage after DNA damage.

Recently, ubiquitination of phosphorylated RPB1 by BRCA1-BARD1 has been reported (23, 25). Because double knockdown of BRCA1 and BARD1 restored the expression level of the phosphorylated polymerase II that had been repressed by UV irradiation, it was proposed that BRCA1-BARD1 could initiate the degradation of stalled RPB1 (23). However, the BRCA1-BARD1 double knockdown did not detectably affect RPB1 ubiquitination after UV

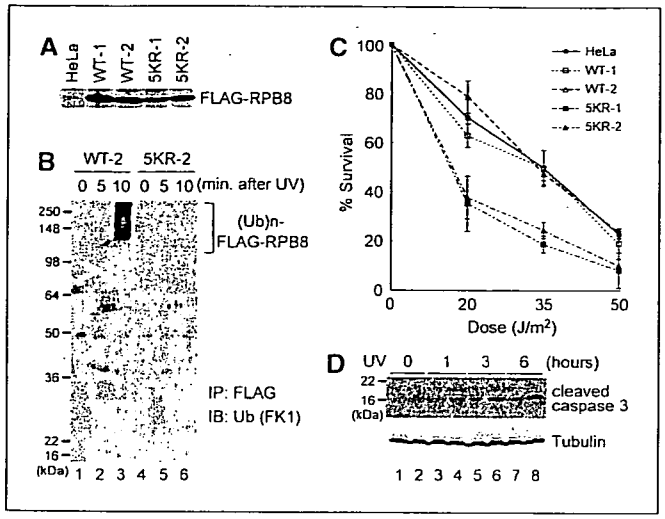

Figure 6. Ubiquitin-resistant RPB8 causes UV hypersensitivity. *A*, cell lysates obtained from two clones each of HeLa cell lines stably expressing either WT (*WT-1* and *WT-2*) or the 5KR mutant (*5KR-1* and *5KR-2*) of FLAG-RPB8 and parental HeLa cells were immunoprecipitated with anti-RPB8 antibody followed by immunoblotting with anti-RPB8 antibody. *B*, HeLa cell lines stably expressing WT (*WT-2, lanes 1–3*) or the 5KR mutant (*5KR-2, lanes 4–6*) of FLAG-RPB8 were UV irradiated (35 J/m^2) and harvested at the indicated times after irradiation. Ubiquitinated RPB8 was detected as described in Fig. 2*B*, except that antipolyubiquitin antibody (*FK1*) was used for immunoblotting. *C*, HeLa cell lines described in *A* were UV irradiated at the indicated doses. Forty-eight hours after irradiation, the cell survival ratio was determined by trypan blue exclusion measurements. The cell number at 0 h (indicated as 0 J/m^2) is 100%. *Points*, mean of measurements carried out in triplicate; *bars*, SD. The experiments were repeated at least twice with similar results. *D*, WT-2 cells (*lanes 1, 3, 5*, and *7*) and 5KR-2 cells (*lanes 2, 4, 6*, and *8*) were UV irradiated (35 J/m^2) and harvested at the indicated times after irradiation. Whole-cell lysates were immunoblotted with anti–caspase-3 antibody or antitubulin antibody.

irradiation. In addition, BRCA1-BARD1–mediated polyubiquitination of other substrates, including NPM1/B23 and phosphorylated CtIP, is not a signal for degradation (12, 33). Therefore, the restored expression level of the phosphorylated polymerase II by BRCA1-BARD1 double knockdown could be due to an indirect effect (23), for example, through the failure to ubiquitinate RPB8. Nonetheless, the clearly shown *in vitro* ubiquitination of phosphorylated RPB1 by BRCA1-BARD1 (23) strongly supports its direct role. The key to solving this discrepancy may be to analyze the timing of RPB1 ubiquitination *in vivo*. RPB1 ubiquitination shown in the previous report occurred 2 h after UV irradiation, when BRCA1 should already be dissociated from polymerase II and relocalized to the Rad50 or Rad51 DNA repair machineries. It is possible that early after DNA damage, RPB1 and RPB8 are transiently ubiquitinated by BRCA1 at the same time, and it may result in dissociation of the polymerase II holoenzyme from the damaged DNA site. RPB1 ubiquitination and degradation occurring in late phases could be mediated by other E3 ligases, such as the CSA-DDB1-CUL4A-ROC1 complex (34, 35).

It is well known that cells with impaired BRCA1 function display hypersensitivity to a range of DNA-damaging agents, including IR and UV irradiation (3, 26). However, the mechanism underlying this phenomenon is not fully understood. Although the failure of checkpoint function is a possible mechanism responsible for the hypersensitivity, it has been reported that neither selective abrogation of the S-phase checkpoint nor the G_2 checkpoint itself results in decreased cell survival after DNA damage (36, 37). Therefore, it has been proposed that some function of BRCA1 other than S-phase or G_2 cell cycle control may affect cell survival after DNA damage (37). The UV hypersensitivity of the cells stably expressing a ubiquitin-resistant mutant of RPB8 shown in this report provides a possible new role for BRCA1 that may compensate for this theoretical defect. Because hyperphosphorylated stalled polymerase II at damaged sites is an extremely cytotoxic ramification of DNA damage (38), the observed UV hypersensitivity could be caused by trapped polymerase II or prolonged polymerase II hyperphosphorylation. In this process, the ubiquitination of RPB8 could be an important step either for polymerase II disassembly, polymerase II dissociation from DNA, or polymerase II dephosphorylation by FCP1. It is interesting that there is considerable expression of endogenous WT RPB8 in the ubiquitin-resistant RPB8 mutant cells (Fig. 4*A*). This indicates that only partial interference of the RNA polymerase recovery is enough to induce cell death, probably by silencing a gene critical for cell survival. Alternatively, polymerase II complexes containing mutant RPB8 could stall at the damaged sites, subsequently causing a gridlock of all polymerase II complexes, including WT complexes. Supporting this idea, induction of local damage by microbeam UV irradiation in the nucleus led to transcription inhibition throughout the nucleus (39).

Lastly, it is noteworthy that RPB8 is shared by all three classes of RNA polymerases (19, 40). Whereas polymerase II synthesizes mRNA, which is only ~ 5% of all RNAs, polymerase I and polymerase III synthesize the remaining 95% of all RNAs. Therefore, modification of those complexes, rather than polymerase II, might enormously influence cellular conditions. Whereas RPB1 has been intensively studied, the role of RPB8 in the DNA damage response has been poorly understood. The ubiquitination of RPB8 by BRCA1 reported here provides additional evidence for the role of RNA polymerases in the DNA damage response as well as in carcinogenesis.

Acknowledgments

Received 8/31/2006; revised 11/15/2006; accepted 11/30/2006.

Grant support: Japan Society for the Promotion of Science and the Japanese Ministry of Education, Culture, Sports, Science and Technology.

The costs of publication of this article were defrayed in part by the payment of page charges. This article must therefore be hereby marked *advertisement* in accordance with 18 U.S.C. Section 1734 solely to indicate this fact.

We thank Drs. Yanping Zhang, Minoru Takata, and Masamichi Ishiai for helpful discussions and critical reading of the manuscript; and Drs. Richard Baer and Nouria Hernandez for their generous contribution of materials.

References

1. Turner N, Tutt A, Ashworth A. Hallmarks of "BRCA-ness" in sporadic cancers. Nat Rev Cancer 2004;4:814–9.
2. Deng CX. Roles of BRCA1 in centrosome duplication. Oncogene 2002;21:6222–7.
3. Venkitaraman AR. Cancer susceptibility and the functions of BRCA1 and BRCA2. Cell 2002;108:171–82.
4. Zheng L, Li S, Boyer TG, Lee WH. Lessons learned from BRCA1 and BRCA2. Oncogene 2000;19:6159–75.
5. Baer R, Ludwig T. The BRCA1/BARD1 heterodimer, a tumor suppressor complex with ubiquitin E3 ligase activity. Curr Opin Genet Dev 2002;12:86–91.
6. Brzovic PS, Keeffe JR, Nishikawa H, et al. Binding and recognition in the assembly of an active BRCA1/BARD1 ubiquitin-ligase complex. Proc Natl Acad Sci U S A 2003;100:5646–51.
7. Hashizume R, Fukuda M, Maeda I, et al. The RING heterodimer BRCA1-1 is a ubiquitin ligase inactivated by a breast cancer-derived mutation. J Biol Chem 2001;276:14537–40.
8. Mallery DL, Vandenberg CJ, Hiom K. Activation of the E3 ligase function of the BRCA1/BARD1

complex by polyubiquitin chains. EMBO J 2002;21: 6755–62.
9. Chau V, Tobias JW, Bachmair A, et al. A multiubiquitin chain is confined to specific lysine in a targeted short-lived protein. Science 1989;243:1576–83.
10. Morris JR, Solomon E. BRCA1: BARD1 induces the formation of conjugated ubiquitin structures, dependent on K6 of ubiquitin, in cells during DNA replication and repair. Hum Mol Genet 2004;13:807–17.
11. Nishikawa H, Ooka S, Sato K, et al. Mass spectrometric and mutational analyses reveal Lys-6-linked polyubiquitin chains catalyzed by BRCA1-1 ubiquitin ligase. J Biol Chem 2004;279:3916–24.
12. Sato K, Hayami R, Wu W, et al. Nucleophosmin/B23 is a candidate substrate for the BRCA1–1 ubiquitin ligase. J Biol Chem 2004;279:30919–22.
13. Wu-Baer F, Lagrazon K, Yuan W, Baer R. The BRCA1/BARD1 heterodimer assembles polyubiquitin chains through an unconventional linkage involving lysine residue K6 of ubiquitin. J Biol Chem 2003;278:34743–6.
14. Ruffner H, Joazeiro CA, Hemmati D, Hunter T, Verma IM. Cancer-predisposing mutations within the RING domain of BRCA1: loss of ubiquitin protein ligase activity and protection from radiation hypersensitivity. Proc Natl Acad Sci U S A 2001;98:5134–9.
15. Chiba N, Parvin JD. The BRCA1 and BARD1 association with the RNA polymerase II holoenzyme. Cancer Res 2002;62:4222–8.
16. Scully R, Anderson SF, Chao DM, et al. BRCA1 is a component of the RNA polymerase II holoenzyme. Proc Natl Acad Sci U S A 1997;94:5605–10.
17. Krum SA, Miranda GA, Lin C, Lane TF. BRCA1 associates with processive RNA polymerase II. J Biol Chem 2003;278:52012–20.
18. Lane TF. BRCA1 and transcription. Cancer Biol Ther 2004;3:528–33.
19. Shpakovski GV, Acker J, Wintzerith M, Lacroix JF, Thuriaux P, Vigneron M. Four subunits that are shared by the three classes of RNA polymerase are functionally interchangeable between *Homo sapiens* and *Saccharomyces cerevisiae*. Mol Cell Biol 1995;15:4702–10.
20. Boulton SJ. BRCA1-mediated ubiquitylation. Cell Cycle 2006;5:1481–6.
21. Kirkpatrick DS, Hathaway NA, Hanna J, et al. Quantitative analysis of *in vitro* ubiquitinated cyclin B1 reveals complex chain topology. Nat Cell Biol 2006;8:700–10.
22. Bregman DB, Halaban R, van Gool AJ, Henning KA, Friedberg EC, Warren SL. UV-induced ubiquitination of RNA polymerase II: a novel modification deficient in Cockayne syndrome cells. Proc Natl Acad Sci U S A 1996; 93:11586–90.
23. Kleiman FE, Wu-Baer F, Fonseca D, Kaneko S, Baer R, Manley JL. BRCA1/BARD1 inhibition of mRNA 3′ processing involves targeted degradation of RNA polymerase II. Genes Dev 2005;19:1227–37.
24. Ratner JN, Balasubramanian B, Corden J, Warren SL, Bregman DB. Ultraviolet radiation-induced ubiquitination and proteasomal degradation of the large subunit of RNA polymerase II. Implications for transcription-coupled DNA repair. J Biol Chem 1998; 273:5184–9.
25. Starita LM, Horwitz AA, Keogh MC, Ishioka C, Parvin JD, Chiba N. BRCA1/BARD1 ubiquitinate phosphorylated RNA polymerase II. J Biol Chem 2005;280:24498–505.
26. Abbott DW, Thompson ME, Robinson-Benion C, Tomlinson G, Jensen RA, Holt JT. BRCA1 expression restores radiation resistance in BRCA1-defective cancer cells through enhancement of transcription-coupled DNA repair. J Biol Chem 1999;274:18808–12.
27. Shen SX, Weaver Z, Xu X, et al. A targeted disruption of the murine Brca1 gene causes γ-irradiation hypersensitivity and genetic instability. Oncogene 1998;17: 3115–24.
28. Greenberg RA, Sobhian B, Pathania S, Cantor SB, Nakatani Y, Livingston DM. Multifactorial contributions to an acute DNA damage response by BRCA1/BARD1-containing complexes. Genes Dev 2006;20:34–46.
29. Cortez D, Wang Y, Qin J, Elledge SJ. Requirement of ATM-dependent phosphorylation of brca1 in the DNA damage response to double-strand breaks. Science 1999; 286:1162–6.
30. Tibbetts RS, Cortez D, Brumbaugh KM, et al. Functional interactions between BRCA1 and the checkpoint kinase ATR during genotoxic stress. Genes Dev 2000;14:2989–3002.
31. Scully R, Chen J, Ochs RL, et al. Dynamic changes of BRCA1 subnuclear location and phosphorylation state are initiated by DNA damage. Cell 1997;90:425–35.
32. Zhong Q, Chen CF, Li S, et al. Association of BRCA1 with the hRad50-11-p95 complex and the DNA damage response. Science 1999;285:747–50.
33. Yu X, Fu S, Lai M, Baer R, Chen J. BRCA1 ubiquitinates its phosphorylation-dependent binding partner CtIP. Genes Dev 2006;20:1721–6.
34. Groisman R, Polanowska J, Kuraoka I, et al. The ubiquitin ligase activity in the DDB2 and CSA complexes is differentially regulated by the COP9 signalosome in response to DNA damage. Cell 2003;113:357–67.
35. Hu J, McCall CM, Ohta T, Xiong Y. Targeted ubiquitination of CDT1 by the DDB1–4A-ROC1 ligase in response to DNA damage. Nat Cell Biol 2004;6: 1003–9.
36. Xu B, Kim ST, Lim DS, Kastan MB. Two molecularly distinct G(2)/M checkpoints are induced by ionizing irradiation. Mol Cell Biol 2002;22:1049–59.
37. Xu B, O'Donnell AH, Kim ST, Kastan MB. Phosphorylation of serine 1387 in Brca1 is specifically required for the Atm-mediated S-phase checkpoint after ionizing irradiation. Cancer Res 2002;62:4588–91.
38. van den Boom V, Jaspers NG, Vermeulen W. When machines get stuck-obstructed RNA polymerase II: displacement, degradation or suicide. Bioessays 2002; 24:780–4.
39. Takeda S, Naruse S, Yatani R. Effects of ultra-violet microbeam irradiation of various sites of HeLa cells on the synthesis of RNA, DNA and protein. Nature 1967;213: 696–7.
40. Briand JF, Navarro F, Rematier P, et al. Partners of Rpb8p, a small subunit shared by yeast RNA polymerases I, II and III. Mol Cell Biol 2001;21: 6056–65.

The EMBO Journal (2007) 26, 113–122 | © 2007 European Molecular Biology Organization | All Rights Reserved 0261-4189/07
www.embojournal.org

THE EMBO JOURNAL

Cytoplasmic destruction of p53 by the endoplasmic reticulum-resident ubiquitin ligase 'Synoviolin'

Satoshi Yamasaki[1,14], Naoko Yagishita[1,14], Takeshi Sasaki[1,14], Minako Nakazawa[1,14], Yukihiro Kato[1,14], Tadayuki Yamadera[1,14], Eunkyung Bae[2,14], Sayumi Toriyama[1], Rie Ikeda[1], Lei Zhang[1], Kazuko Fujitani[1], Eunkyung Yoo[2], Kaneyuki Tsuchimochi[1], Tomohiko Ohta[3], Natsumi Araya[1], Hidetoshi Fujita[1], Satoko Aratani[1], Katsumi Eguchi[4], Setsuro Komiya[5], Ikuro Maruyama[6], Nobuyo Higashi[7], Mitsuru Sato[7], Haruki Senoo[7], Takahiro Ochi[8], Shigeyuki Yokoyama[9], Tetsuya Amano[1], Jaeseob Kim[2], Steffen Gay[10], Akiyoshi Fukamizu[11], Kusuki Nishioka[12], Keiji Tanaka[13] and Toshihiro Nakajima[1,*]

[1]Department of Genome Science, Institute of Medical Science, St Marianna University School of Medicine, Kawasaki, Japan, [2]GenExl, Inc. Biomedical Research Center, Taejon, South Korea, [3]Division of Breast and Endocrine Surgery, Institute of Medical Science, St Marianna University School of Medicine, Kawasaki, Japan, [4]The First Department of Internal Medicine, Nagasaki University School of Medicine, Nagasaki, Japan, [5]Department of Orthopedic Surgery, Kagoshima University, Faculty of Medicine, Kagoshima, Japan, [6]Department of Dermatology and Laboratory of Molecular Medicine, Kagoshima University, Faculty of Medicine, Kagoshima, Japan, [7]Department of Anatomy, Akita University School of Medicine, Akita, Japan, [8]National Hospital Organization Sagamihara National Hospital, Kanagawa, Japan, [9]Department of Biophysics and Biochemistry, Graduate School of Science, University of Tokyo, Tokyo, Japan; Protein Research Group, RIKEN Genomic Sciences Center, Yokohama, Japan, [10]Department of Rheumatology, University Hospital Zürich, Zürich, Switzerland, [11]Aspect of Functional Genomic Biology, Center of Tsukuba Advanced Research Alliance, University of Tsukuba, Tsukuba, Japan, [12]Rheumatology, Immunology and Genetics Program, Institute of Medical Science, St Marianna University School of Medicine, Kawasaki, Japan and [13]Laboratory of Frontier Science, The Tokyo Metropolitan Institute of Medical Science, Tokyo, Japan

Synoviolin, also called HRD1, is an E3 ubiquitin ligase and is implicated in endoplasmic reticulum -associated degradation. In mammals, Synoviolin plays crucial roles in various physiological and pathological processes, including embryogenesis and the pathogenesis of arthropathy. However, little is known about the molecular mechanisms of Synoviolin in these actions. To clarify these issues, we analyzed the profile of protein expression in *synoviolin*-null cells. Here, we report that Synoviolin targets tumor suppressor gene p53 for ubiquitination. Synoviolin sequestrated and metabolized p53 in the cytoplasm and negatively regulated its cellular level and biological functions, including transcription, cell cycle regulation and apoptosis. Furthermore, these p53 regulatory functions of Synoviolin were irrelevant to other E3 ubiquitin ligases for p53, such as MDM2, Pirh2 and Cop1, which form autoregulatory feedback loops. Our results provide novel insights into p53 signaling mediated by Synoviolin.

The EMBO Journal (2007) **26,** 113–122. doi:10.1038/sj.emboj.7601490; Published online 14 December 2006
Subject Categories: proteins
Keywords: apoptosis; cell growth; E3 ubiquitin ligase; endoplasmic reticulum-associated degradation; rheumatoid arthritis

Introduction

The ubiquitin–proteasome system (UPS) consists of a small polypeptide ubiquitin, a framework of enzymes that mediates the covalent attachment of ubiquitin to proteolytic substrates and the 26S proteasome that digests the modified proteins into peptides. The formation of ubiquitin conjugates requires the successive action of three classes of enzymes. This process is first activated by an E1 (activating enzyme) in an ATP-dependent manner, forming a high-energy thioester bond between ubiquitin and an E1, and the activated ubiquitin is then transferred to an E2 (conjugating enzyme), forming a similar thioester linkage between ubiquitin and E2, and then E3 ubiquitin ligase transfers ubiquitin to the target proteins. Through repeated reactions of this cycle, a polyubiquitin chain is formed on the target proteins, which is recognized by the 26S proteasome for ultimate degradation (Hershko and Ciechanover, 1998; Pickart, 2001). In the UPS pathway, the E3 ubiquitin ligases play critical roles in the selection of target proteins for degradation, because each distinct E3 ubiquitin ligase usually binds a protein substrate with a degree of selectivity for ubiquitination in a temporally and spatially regulated fashion.

Synoviolin, a representative of endoplasmic reticulum (ER)-resident E3 ubiquitin ligases, is a mammalian homolog of Hrd1p/Der3p that "substrates" misfolded carboxypeptide yscY (CPY*) (Bordallo *et al*, 1998) and 3-hydroxy-3-methylglutaryl-coenzyme A reductase (HMGR), a key enzyme of the mevalonate pathway in yeast (Shearer and Hampton, 2004, 2005). We cloned Synoviolin from rheumatoid synovial cells (RSCs) and described that Synoviolin is highly expressed in synoviocytes of patients with rheumatoid arthritis (RA) (Amano *et al*, 2003). In that report, we demonstrated that overexpression of Synoviolin in transgenic mice leads to advanced arthropathy caused by reduced apoptosis of synoviocytes. On the other hand, *synoviolin*$^{+/-}$ mice showed resistance to the development of arthritis owing to enhanced

*Corresponding author. Department of Genome Science, Institute of Medical Science, St Marianna University School of Medicine, 2-16-1 Sugao Miyamae-ku, Kawasaki, Kanagawa 216-8512, Japan. Tel.: +81 44 977 8111 (ext. 4111); Fax: +81 44 977 10712; E-mail: nakashit@marianna-u.ac.jp
[14]These authors contributed equally to this work

Received: 11 April 2006; accepted: 7 November 2006; published online: 14 December 2006

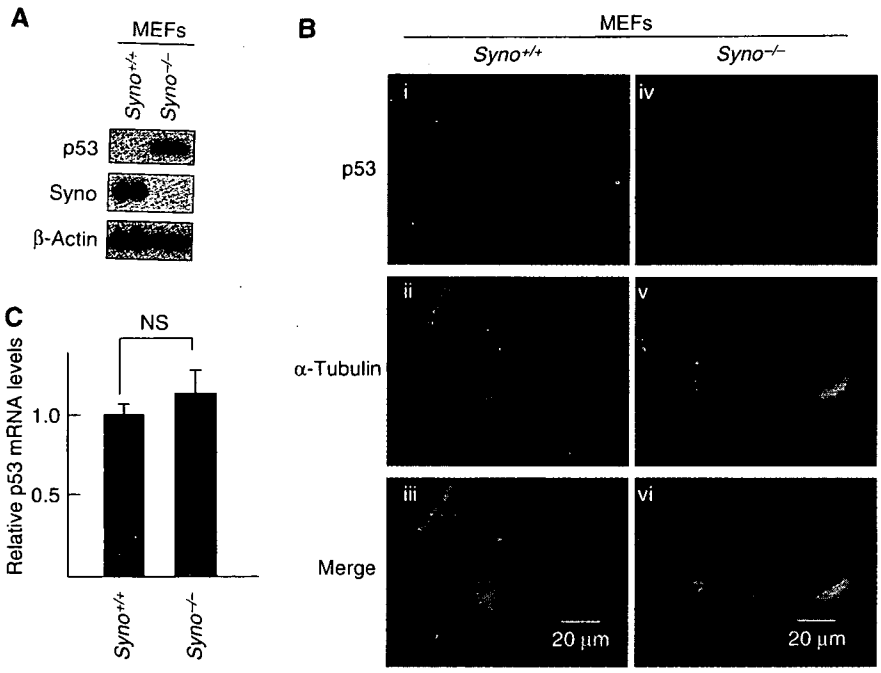

Figure 1 Accumulation of p53 in *synoviolin* null cells. (**A**) Accumulation of p53 in *Syno*$^{-/-}$ MEFs. (**B**) Nuclear accumulation of p53 in *Syno*$^{-/-}$ MEFs. p53 in *Syno*$^{+/+}$ MEFs (i–iii) and *Syno*$^{-/-}$ MEFs (iv–vi). Merged images are shown in the bottom panels (iii, vi). (**C**) Quantification of p53 mRNA. The *p53* mRNA level was assessed by real-time PCR and normalized to 18S rRNA. Data are mean±s.e.m. of four experiments. Statistical analysis using Student *t*-test indicated no significant difference between *Syno*$^{+/+}$ and *Syno*$^{-/-}$ MEFs (NS).

apoptosis of synovial cells. These results indicate that Synoviolin is a novel causative factor for arthropathy based on its anti-apoptotic effects. In another study, we reported that all mice fetuses lacking *synoviolin* (*Syno*$^{-/-}$) died *in utero* around E13.5 (Yagishita *et al*, 2005), although Hrd1p/Del3p, a yeast ortholog of Synoviolin, was described as non-essential for survival. *Syno*$^{-/-}$ were anemic owing to enhanced apoptosis of fetal liver cells (Yagishita *et al*, 2005). It is surprising that an ER-associated degradation (ERAD)-associated E3 ubiquitin ligase, Synoviolin, is involved in cell hyperplasia of dividing cells via its anti-apoptotic effect. In this regard, like RSCs, the anti-apoptotic effect of Synoviolin was observed even for *synoviolin* expressed ectopically in NIH3T3 cells, which resulted in enhanced cell overgrowth in these cells (Tsuchimochi *et al*, 2005). These results were confirmed also in the *Drosophila* fly (Supplementary Figure 1). An important question remains unanswered at this stage. What is the mechanism of Synoviolin-induced cell overgrowth? The present study was designed to identify the substrates for Synoviolin that may be involved in cell growth.

Results

Accumulation of p53 in synoviolin-null cells

To identify target(s) for Synoviolin, we assumed that the lack of Synoviolin results in accumulation of substrate proteins. First, we carried out a two-dimensional polyacrylamide gel electrophoresis (PAGE) using mouse embryonic fibroblasts (MEFs) of *Syno*$^{-/-}$. In these experiments, p53 was identified as one of the major targets in the profile by LC-MAS analysis (Supplementary Figure 2). Indeed, the level of p53 was markedly enhanced in *Syno*$^{-/-}$ MEFs (Figure 1A) and *Syno*$^{-/-}$ embryos, especially in the posterior part of the body such as somites, brains and maxillary or branchial arches (Supplementary Figure 3), as reported previously (Gottlieb *et al*, 1997). The accumulated p53 was predominantly localized in the nuclei of *Syno*$^{-/-}$ MEFs (Figure 1B), although the mRNA level of *p53* was not altered in *Syno*$^{-/-}$ MEFs (Figure 1C). Phosphorylation of p53 was not observed in *Syno*$^{-/-}$ MEFs (Supplementary Figure 4).

Increment of functional p53 in synoviolin-null cells

Next, we tested whether impairment of Synoviolin influences the functions of p53 in the cell. Knockdown of Synoviolin by small interfering RNA (siRNA) for *synoviolin* (*Syno* siRNA) in RKO cells, a human colon cancer cell line known to express wild-type (WT) p53 (Smith *et al*, 1995), resulted in almost complete disappearance of Synoviolin expression (Figure 2A). Synoviolin knockdown was associated with increased p53 protein level and nuclear accumulation of p53 (Figure 2A and B), but no change in p53 mRNA levels (Figure 2C). No changes were noted in the expression levels of other ubiquitin ligases for p53 such as MDM2, Arf-BP (data not shown) and Parc (see Figure 4B), in *synoviolin*-null RKO cells (Brooks and Gu, 2006). On the other hand, the expression levels of unfolded protein response (UPR) markers such as HERP and PERK (Wu and Kaufman, 2006) were increased, which suggests that accumulation of unfolded proteins in *synoviolin*-knockdown RKO cells caused ER stress, followed by UPR (data not shown). These results were confirmed in other cell lines (HEK293 cells and HeLa cells, data not shown). In another experiment, a marked increase was noted in the binding of p53 to its consensus sequences such as *GADD45*, *MDM2* and *p21* promoter in *synoviolin*-knockdown cells compared with *GFP*-knockdown cells (Figure 2D). Furthermore, further additions of the respective competitor abrogated the binding capacity dose-dependently, confirming the specific interactions of p53 on electrophoretic mobility

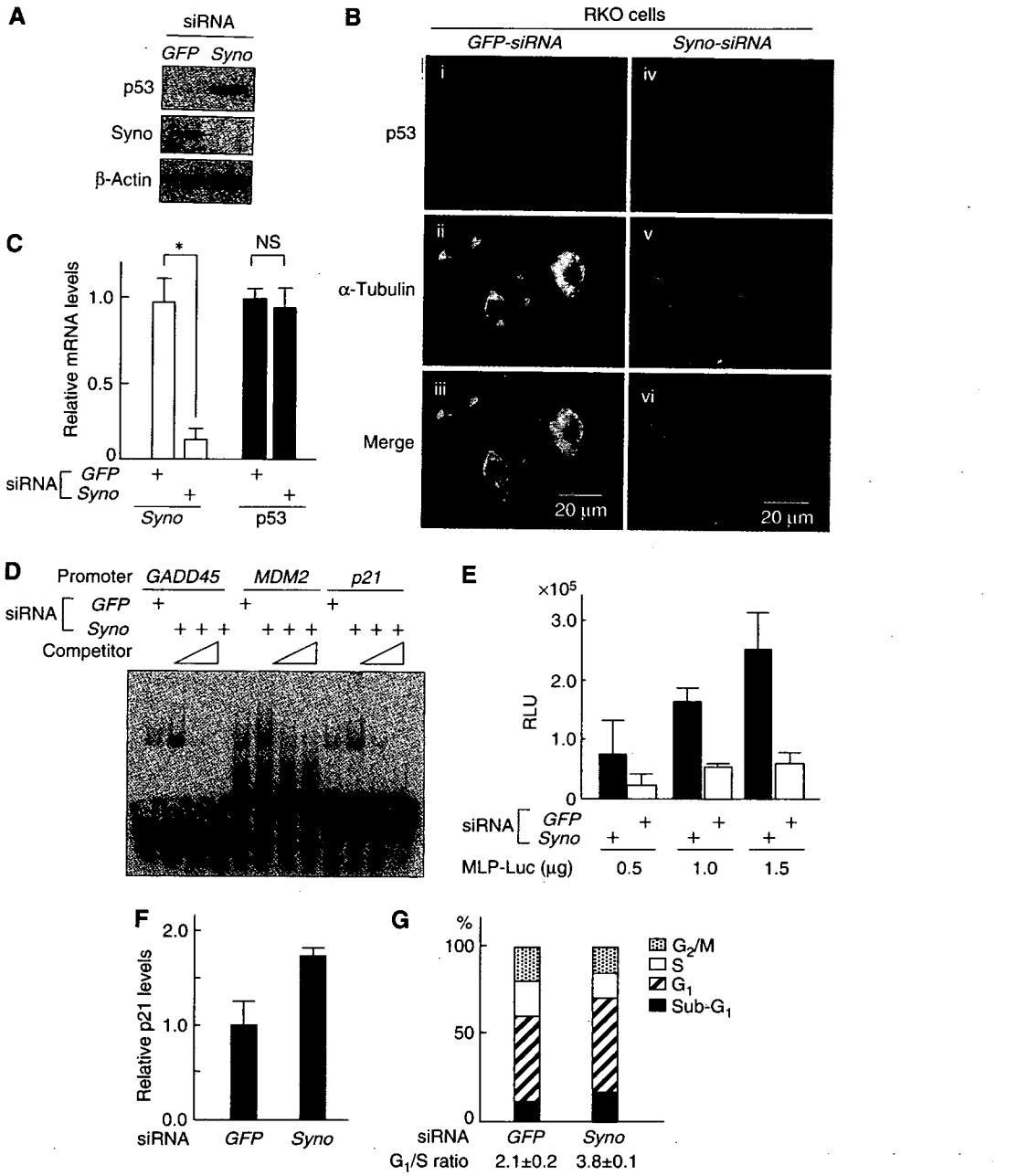

Figure 2 Functional evaluation of increased p53 in *synoviolin*-deficient RKO cells. (**A**) Increment of endogenous p53 by depletion of *synoviolin*. (**B**) Depletion of *synoviolin* causes nuclear accumulation of p53. Merged images are shown in the bottom panels (iii, vi). (**C**) *synoviolin* depletion does not affect mRNA levels of *p53*. Real-time PCR was performed as in Figure 1C. $^*P<0.01$. (**D**) DNA-binding activity of p53 for promoters of the indicated genes increases by depletion of *synoviolin*. (**E**) Transactivation activity of p53 is increased upon depletion of Synoviolin. Relative transactivation activity was determined by normalizing luciferase to an internal control, β-Gal activity from RSV-β-gal plasmid. RLU, relative light units. (**F**) siRNA depletion of *synoviolin* causes activation of p21 expression. (**G**) siRNA-induced depletion of *synoviolin* induces G_1 arrest. The cell-cycle profile was determined by propidium iodide staining and FACS. The results represent the average of triplicate experiments. Data in (C), (E) and (F) are mean±s.e.m. of four experiments.

shift assay (EMSA) (Figure 2D). We also noted three times increment of luciferase activities on *GADD45*-MLP-Luciferase reporter plasmid in *synoviolin*-deficient RKO cells compared with *GFP*-siRNA-treated RKO cells (Figure 2E). Moreover, in *Syno* siRNA-treated RKO cells, we detected enhanced expression of p21, one of the target genes of p53 (Figure 2F), and the accumulation of cells in G_1 phase and decreased cells in S phase (Figure 2G). Taken together, the above results indicate that Synoviolin deficiency is not only associated with increased levels of p53, but also with functional activation of p53.

Synoviolin sequestrates p53 in the cytoplasm

To understand the molecular mechanism of Synoviolin-induced control of p53, we investigated the interaction between Synoviolin and p53 *in vitro*. As shown in Figure 3A, GST-SynoΔTM interacted directly with p53 (lane 8). A series of N-terminus Synoviolin-TM deletion mutants showed that the amino-acid sequence 236–270 of Synoviolin is responsible for binding with p53 (lanes 1–6) (this binding domain was termed provisionally as '53BD'). Furthermore, a synthetic 53BD peptide inhibited Synoviolin-p53 interaction in a dose-

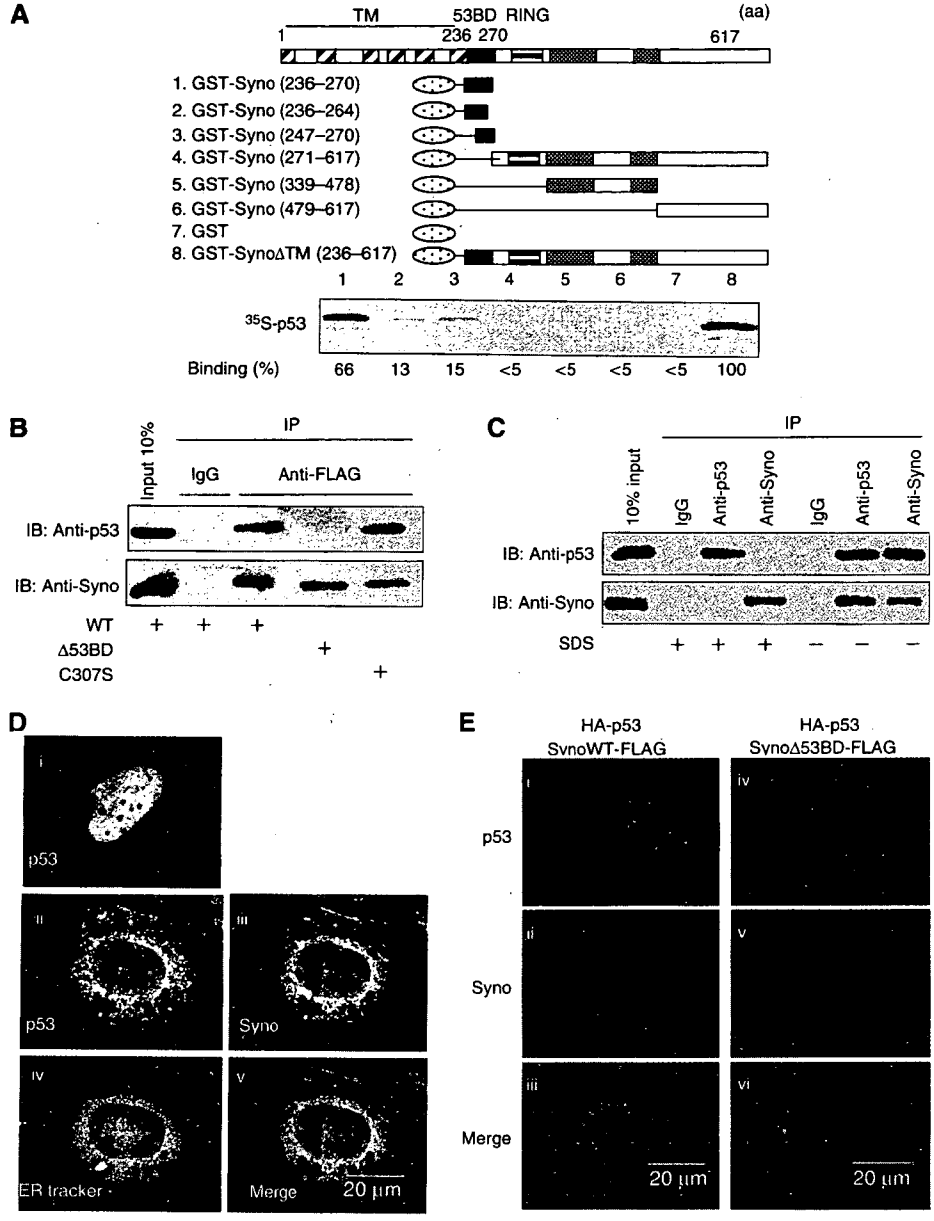

Figure 3 Synoviolin sequestrates p53 in the ER through its 53BD-dependent interaction with p53. (**A**) Identification of p53-binding domain of Synoviolin *in vitro*. Black box: p53-binding domain (53BD), gray box: proline-rich domain, oval box: GST. Relative binding ability is denoted as percentage (100% = SynoΔTM, lane 8). (**B**) 53BD-dependent *in vivo* binding of Synoviolin with p53 in HEK293 cell. (**C**) Interaction between endogenous Synoviolin and p53 in HEK293 cells. Cell lysates were immunoprecipitated in the presence or absence of SDS by using anti-p53 antibodies, anti-Synoviolin antibodies or control IgG. Inputs and immunoprecipitates were analyzed by Western blot by using anti-p53 or anti-Synoviolin antibodies. (**D**) P53 is anchored around ER in a Synoviolin-dependent manner. Saos-2 cells were transfected with HA-p53 (i) or co-transfected with HA-p53 and Synoviolin-FLAG (ii–v). Panel v shows a merged image with p53 (green), Synoviolin (red) and ER-Tracker stain (blue). (**E**) Binding of p53 with Synoviolin is required for p53 anchoring in the ER. Saos-2 cells were co-transfected with HA-p53 and Synoviolin WT-FLAG (I–iii) or SynoviolinΔ53BD-FLAG (iv–vi). Merged images are shown in the bottom panels (iii, vi).

dependent manner, whereas a peptide representing amino acids 322–332 of Synoviolin, used as a negative control, did not show any inhibitory activity (Supplementary Figure 5). We also confirmed *in vivo*, using co-immunoprecipitation assay, the interaction of transiently expressed exogenous Synoviolin WT-FLAG and p53, and the necessity of 53BD was also apparent (Figure 3B). The interaction of these two molecules was independent of ubiquitin ligase activity of Synoviolin, because Synoviolin C307S-FLAG lacking E3 activity bound to p53, as its WT (Figure 3B). Furthermore, endogenous interaction of p53 and Synoviolin was also confirmed in HEK293 cells (Figure 3C).

Considering the interplay between the ER-resident Synoviolin and the nuclear p53, we next investigated their cellular localization in Saos-2 cells, a human osteosarcoma cell line that lacks the endogenous p53 gene (Fogh *et al*, 1977), under conditions of transient expression of exogenous HA-p53 with Synoviolin WT-FLAG or SynoviolinΔ53BD-FLAG (Figure 3D and E). By overexpression of HA-p53 alone in these cells, HA-p53 was localized in the nucleus (Figure 3Di), as reported previously (Shaulsky *et al*, 1990). On the other hand, when HA-p53 was coexpressed with Synoviolin WT-FLAG, HA-p53 was predominantly colocalized with Synoviolin WT-FLAG in the perinuclear regions, but not in

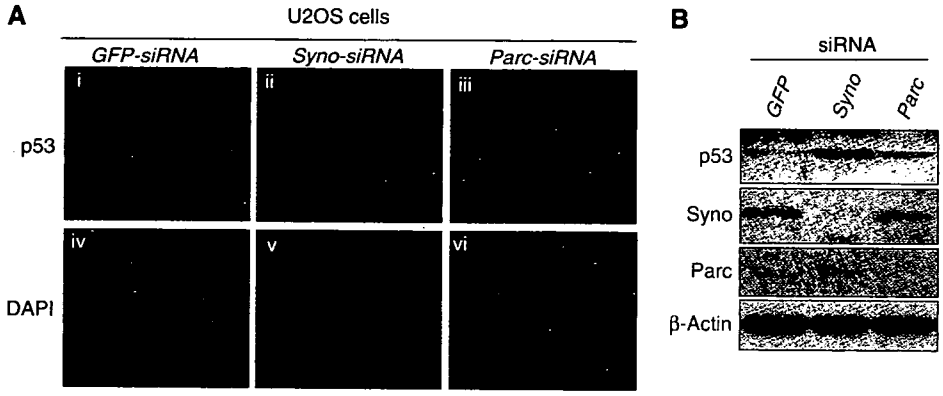

Figure 4 p53-related functional differences between Synoviolin and Parc. (**A**) Nuclear accumulation of p53 by knockdown of *synoviolin* or *Parc*. (**B**) Different levels of p53 following knockdown of *synoviolin* compared with *Parc*.

the nucleus (Figure 3Dii, iii and v). The perinuclear regions were confirmed to be the ER, by counterstaining with ER-Tracker Blue-White DPX (Figure 3Div and v). In addition, ectopically expressed SynoviolinΔ53BD-FLAG did not affect the translocation of HA-p53 into the nucleus (Figure 3E). These results clearly indicate that Synoviolin entraps p53 around ER, and that 53BD is required for this sequestration *in vivo*. In this regard, a previous study reported that another RING finger protein, Parc (Nikolaev *et al*, 2003), also acts as a cytoplasmic anchor for p53. To compare the characteristics of Synoviolin and Parc, we investigated p53 localization in U2OS cells, a human osteosarcoma cell line known to express WT p53 (Ponten and Saksela, 1967), after depletion of *synoviolin* or *Parc* (Nikolaev *et al*, 2003). Treatment with either *Syno* siRNA (Figure 4Aii and v) or *Parc* siRNA (Figure 4Aiii and vi) resulted in accumulation of p53 in the nucleus with diffused and lesser staining in the cytoplasm, different from treatment with *GFP* siRNA. Whereas the nuclear translocation of p53 was comparable in both *Syno* siRNA and *Parc* siRNA cells, a higher expression of p53 was observed in *synoviolin*-deficient U2OS cells (Figure 4Aii and iii). Western blotting analysis also revealed increased level of p53 in Synoviolin-knockdown but not in Parc-knockdown cells (Figure 4B). These findings indicate that Synoviolin regulates both localization and quantity of p53, whereas Parc does not affect the amount of p53, as reported previously (Nikolaev *et al*, 2003).

Synoviolin functions as a novel E3 ubiquitin ligase for p53 degradation

Considering that Synoviolin interacts with p53 *in vitro* and *in vivo*, we next examined whether Synoviolin ubiquitinates p53. As shown in Figure 5A, polyubiquitinated GST-p53 was detected only in the presence of ATP, PK-His-HA-Ub, E1, E2 (UbcH5c) and SynoviolinΔTM (SynoΔTM). This activity was not observed when we used Synoviolin with mutation in the RING finger domain (Figure 5B), and the deletion of 53BD also did not show any ubiquitination activity on p53 (Figure 5B), but this mutant by itself still preserved the auto-ubiquitination activity (Supplementary Figure 6). In addition, the 53BD peptide also inhibited poly-ubiquitination of p53 compared with a control peptide (amino acids 322–332), although the 53BD peptide did not influence the auto-ubiquitination activity of Synoviolin (Supplementary Figure 7). Moreover, ubiquitinated FLAG-p53 was observed when HA-tagged ubiquitin and Synoviolin WT were coexpressed in HEK293 cells because of its easy transfection, but Synoviolin C307S did not (Figure 5C). As a positive control, p53 was ubiquitinated by MDM2 in an *in vivo* ubiquitination assay (Figure 5C) (Haupt *et al*, 1997; Kubbutat *et al*, 1997).

In the next step, we tested the implication of ubiquitination of p53 by Synoviolin in the degradation of p53 *in vivo*. In HEK293 cells, overexpressed Synoviolin WT significantly shortened the half-life of endogenous p53, whereas Synoviolin C307S and SynoviolinΔ53BD did not increase the degradation rate of p53 (Figure 5D top, mock: 125.5± 18.2 min, Synoviolin WT: 44.8±3.8 min, Synoviolin C307S: 177.3±26.8 min and SynoviolinΔ53BD: 161.0±41.4 min). These results indicate that Synoviolin is responsible for the turnover of p53 as its E3 ubiquitin ligase *in vivo*. Consistent with these data, the half-life of p53 was significantly prolonged in $Syno^{-/-}$ MEFs (Figure 5D (bottom), $Syno^{+/+}$ MEFs: 26.1±1.6 min; and $Syno^{-/-}$ MEFs: 120.0±30.3 min. $P<0.05$) as well as RKO cells treated with *synoviolin* siRNA (Supplementary Figure 8). In this regard, several ubiquitin ligases, such as *Cop1* (Dornan *et al*, 2004), *Pirh2* (Leng *et al*, 2003) and *MDM2* (Haupt *et al*, 1997; Kubbutat *et al*, 1997), are already reported to negatively regulate p53 (Bode and Dong, 2004). To ascertain the significance of Synoviolin relative to these ligases, we compared the effects of depletion of *synoviolin* and/or *Cop1*, *Pirh2* or *MDM2* on the expression level of p53 in RKO cells. The amount of p53 by *synoviolin* ablation was less than that by *MDM2* ablation, but equivalent to that by *Cop1* ablation. Depletion of *synoviolin* in cells treated with siRNA for *Cop1*, *Pirh2* or *MDM2* non-redundantly increased p53 levels (Figure 5E). Therefore, Synoviolin functionally targets p53 independent of other ubiquitin ligase pathways. Then, does Synoviolin regulate p53 activation process? To address this question, we applied genotoxic stress as a stimulus for p53 activation (Kastan *et al*, 1991; Vogelstein *et al*, 2000). *Syno* siRNA and *GFP* siRNA-transfected RKO cells were treated with or without genotoxic stresses such as camptothecin, actinomycin D and γ-irradiation. As expected, increased level of p53 by Synoviolin knockdown was cooperatively enhanced by treatment with genotoxic stresses in these cells (Figure 5F). Thapsigargin induced Synoviolin expression, as reported previously (Yagishita *et al*, 2005),

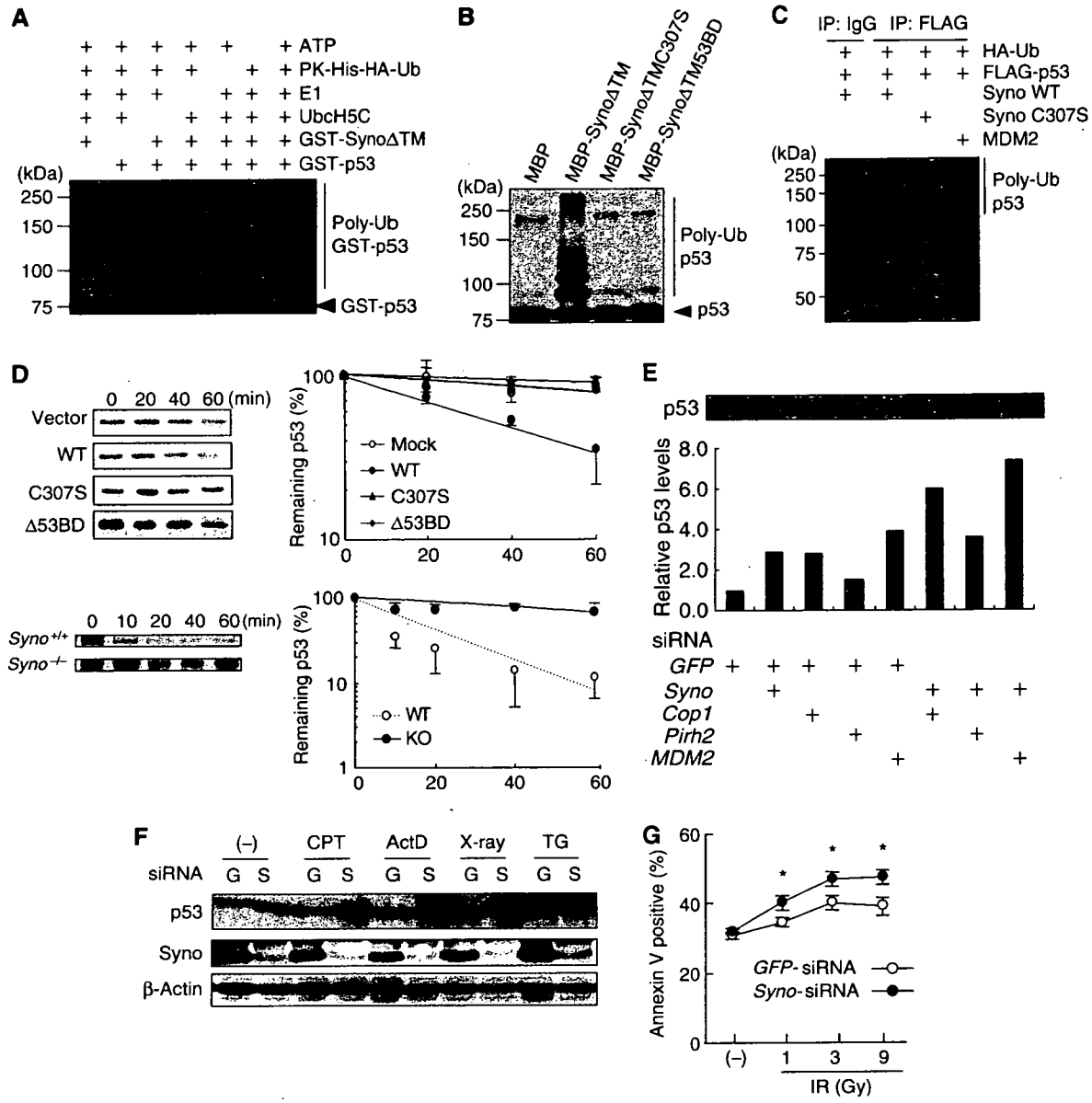

Figure 5 Synoviolin up-regulates p53 level in cells under normal and genotoxic stress conditions. (**A**) Synoviolin ubiquitinates p53 *in vitro*. (**B**) The ubiquitination of p53 is dependent on an intact RING finger domain. (**C**) WT Synoviolin, but not RING finger mutant, ubiquitinates p53 *in vivo*. (**D**) Synoviolin over-expression in HEK293 cells increases degradation of p53 (top). At 24 h after the transfection with empty vector, wild type Synoviolin (WT), mutants in RING finger domain (C307S) or p53 binding domain deletion mutant (Δ53BD), p53 expression was examined at indicated time of cycloheximide treatment. Degradation of p53 is inhibited in synoviolin knockout MEFs ($Syno^{-/-}$) compared with wild type MEFs ($Syno^{+/+}$). The p53 expression was examined after the indicated time of cycloheximide treatment. The remaining p53 expressions were normalized to β-actin expression and plotted against time (minutes). (**E**) Effects of knockdown of Synoviolin and/or other known E3 ubiquitin ligases for p53 on the level of p53 in RKO cells. Quantified p53 level is expressed as relative levels (1.0 = *GFP*-siRNA treated RKO cells). (**F**) Genotoxic stress induces p53 accumulation in the absence of Synoviolin. *GFP*- siRNA (G). *syno* siRNA (S). At 48 h after transfection, the RKO cells were treated with vehicle, camptothecine (CPT, 0.5 μM), actinomycin D (ActD, 5 nM), X-Ray (9 Gray) or thapsigargin (TG, 1 μM) for 6 h. (**G**) Synoviolin knockdown sensitizes cells to genotoxic stress. At 48 h after transfection, cells were exposed to the indicated doses of ionizing-radiation for 24 h, followed by FACS analysis to detect annexin V-positive cells. Data in (D) and (G) are mean ± s.e.m. of $n \geqslant 3$. $^*P<0.05$.

which was abolished in *Syno* siRNA-transfected RKO cells (Figure 5F). Consistent with the findings of a previous report (Qu *et al*, 2004), thapsigargin, an ER stress inducer, destabilized p53 expression compared with vehicle treatment in *GFP* siRNA-treated RKO cells. Interestingly, the thapsigargin-induced inhibition of p53 expression was reversed, at least in part, by the ablation of Synoviolin (Figure 5F). In addition, the sensitivity of *syno* siRNA-treated RKO cells to γ-irradiation was significantly increased compared with *GFP* siRNA-treated RKO cells (Figure 5G). Considered together, these results indicate that Synoviolin also participates in genotoxic stress response through the mechanism identified here.

Synoviolin regulates p53-dependent apoptotic pathway in vivo

The above experiments provided several pieces of evidence that Synoviolin is a novel class of E3 ubiquitin ligase for p53. However, the majority of the results obtained from cultured cells may not fully reflect the physiological function of p53 in

the context of the whole organism. Therefore, we used *Drosophila* to confirm the association between Synoviolin and p53. Among *Drosophila* clones, CG1937 was identified by BLASTP (protein–protein blast analysis using flybase—http://flybase.bio.indiana.edu/blast/) as the gene with 63% homology to mammalian Synoviolin, and the RING domain of CG1937 is highly conserved (82%) and *in vitro* ubiquitination assay evidently indicated that *Drosophila* Synoviolin (dSyno) ubiquitinates *Drosophila* p53 (Dmp53) (Figure 6A) (Ollmann *et al*, 2000). To investigate the role of Synoviolin in p53 regulation in the whole organism, we generated transgenic flies in which Dmp53 or dSyno was overexpressed by tissue-specific Gal4 driver (Harrison *et al*, 1995). By crossing each transgenic fly, we generated e16E-Gal4/UAS-Dmp53;UAS-dSyno/+ flies, in which both Dmp53 and dSyno could be overexpressed in the posterior halves of wings by e16E-Gal4 driver. The expression level of Dmp53 in the wing discs was significantly decreased in e16E-Gal4/UAS-Dmp53;UAS-dSyno/+ discs compared with e16E-Gal4/Dmp53;+/+ discs (Figure 6B). Moreover, acridine orange staining of apoptotic cells in these discs demonstrated that the level of apoptosis induced by overexpression of Dmp53 was diminished by dSyno overexpression (Figure 6C). These results indicate that dSyno affects Dmp53 protein levels in the fly system, similar to the results of the cell culture system.

In addition to decreased Dmp53 protein level by dSyno in the wing discs of adult flies, dSyno altered the wing phenotype. Namely, overexpression of Dmp53 by e16E-Gal4 driver caused bubbled wing phenotype at the posterior half of wings (Figure 6Di). This phenotype was completely suppressed by dSyno overexpression (Figure 6Dii and Supplementary Table 1). Overexpression of dSyno alone by e16E-Gal4 driver also produced wing phenotype (weak wrinkling of the posterior edge of the wing) (Figure 6Diii). This wrinkled phenotype

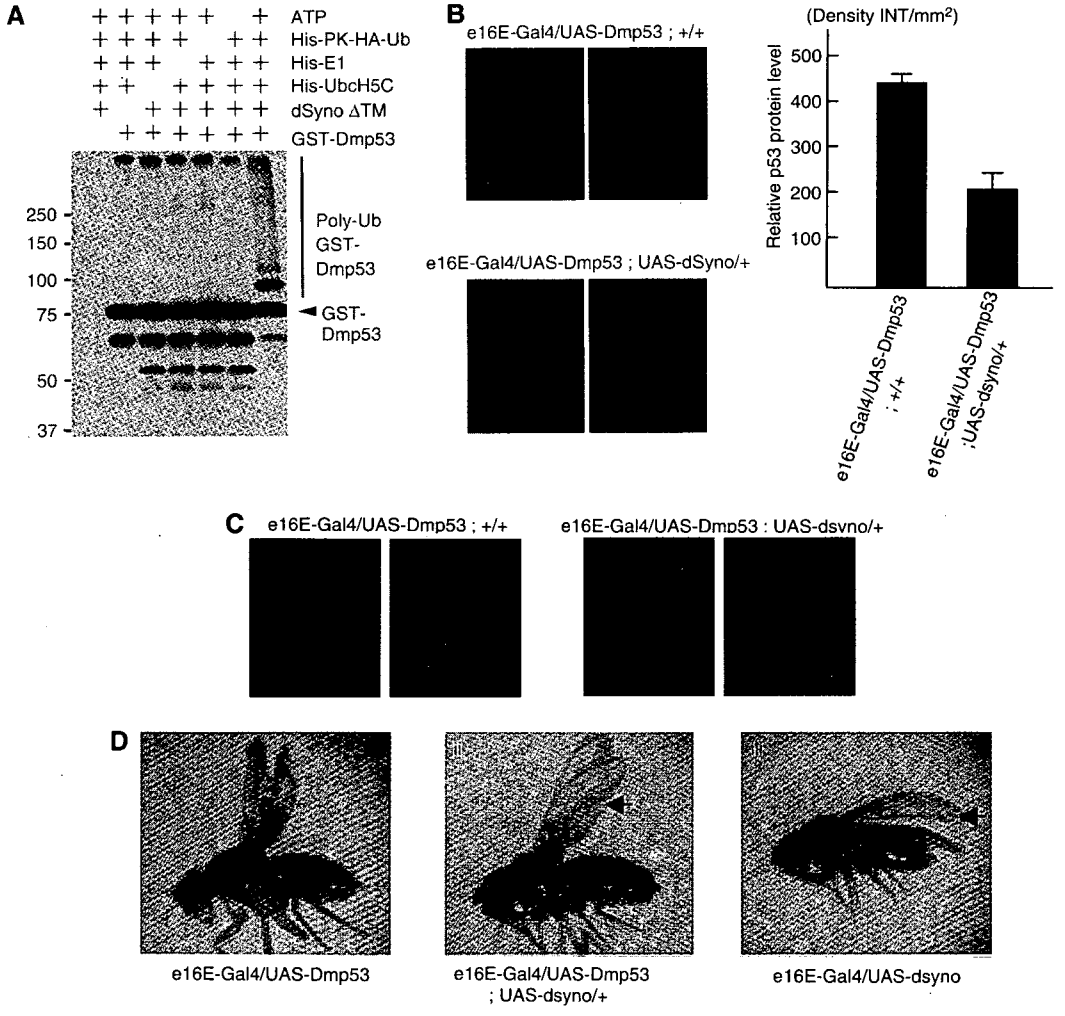

Figure 6 Synoviolin directly regulates p53-dependent apoptotic pathway in *Drosophila* fly. (**A**) Fly homolog of Synoviolin ubiquitinates fly homolog of p53 *in vitro*. GST-fusion *Drosophila melanogaster* p53 (Dmp53) was incubated with or without ATP, His-PK-HA-Ub, His-E1 (human), His-UbcH5C (human) and *Drosophila* Synoviolin (dSyno)ΔTM. Ubiquitinated proteins were probed with anti-HA antibody. (**B**) P53 protein level of wing discs was determined by immunostaining using anti-Dmp53 antibody (left). 2 representative pictures of each fly are shown. The fluorescence intensity of each 15 fly disc was quantified, and the net density level (Density INT/mm^2) was determined by subtracting the density level of the background area (anterior half of disc) from the measured level of the target area (posterior half of disc) (right). Data are mean ± s.e.m. of $n = 15$. (**C**) Apoptosis was examined by Acridine orange staining of wing disc. Overexpression of dSyno in the posterior half of the discs reduced Dmp53 overexpression-induced apoptosis. (**D**) Overexpression of dSyno suppressed the Dmp53-induced bubbled wing phenotype. The extent of wing bubble (*) in e16E-Gal4/UAS-Dmp53 flies varied with age, but the penetrance of bubbled wing phenotype was close to 100% (Supplementary Table 1). Overexpression of dSyno suppressed the Dmp53-induced bubbled wing phenotype, but dSyno-induced wrinkled phenotype at the posterior edge of wing was still observed (arrow).

induced by dSyno overexpression was not affected by Dmp53 in the double overexpressing flies (Figure 6Dii and iii, arrow). These results confirm that dSyno regulates Dmp53 protein level *in vivo* and such regulation might be accomplished through ubiquitination of dDmp53.

To determine whether this phenotypic suppression of Dmp53 by dSyno is specific to Dmp53, we investigated the interaction between dSyno and the upstream activators of p53 such as dATM, CHK2, using the same strategy. None of these activators showed interaction with dSyno (data not shown), suggesting that dSyno regulates Dmp53 protein level directly *in vivo*.

Discussion

We provide concrete evidence for the first time of the functional relationship between Synoviolin and p53. As a target for Synoviolin, p53 is evidently a non-ERAD substrate. In this regard, Doa10p, the RING finger E3 ubiquitin ligase, is known not only to be involved exclusively in removing ER proteins in the ERAD, but also to eliminate cytoplasmic targets, especially the soluble transcriptional factor Matα2, which translocates into the nucleus similar to p53 (Swanson *et al*, 2001; Laney and Hochstrasser, 2003). Thus, our finding can be viewed within the same framework of yeast though in higher eukaryotes. In the meantime, it was proposed that the ERAD in yeast is composed of two distinct surveillance mechanisms, that is, the folded state of luminal domains and the cytosolic domains are monitored by ERAD-luminal (ERAD-L) and ERAD-cytosolic (ERAD-C) pathways, respectively (Vashist and Ng, 2004; Nishikawa *et al*, 2005). Hrd1p is recognized as an ERAD-L ligase; however, this classification is not applicable to Synoviolin as a human homolog of yeast Hrd1, because Synoviolin can target both ERAD-L substrate and cytoplasmic p53 (ERAD-C substrate). Therefore, we propose the novel regulatory system of Synoviolin as a different classification of the ERAD-L/C pathway.

Maintenance of homeostasis is an important cellular function, and cells are equipped with various processes to maintain their conditions. Transcriptional alteration mediated by p53 results in a variety of cell fate changes, including growth arrest and apoptosis (Vousden and Lu, 2002; Meek, 2004). Normally, the cell maintains low levels of p53 through rapid protein degradation via the UPS by the function of ubiquitin ligases. In contrast, under genotoxic stress conditions, stabilization of p53 is promoted and the diffusely distributed p53 translocates to the nucleus owing to growth inhibition and apoptosis by its transcriptional activity. Thus, adjusting the level and nuclear localization of p53 are two essential processes for cells in order to maintain the physiological state. Although p53 mutations have been documented in more than half of all human tumors (Hollstein *et al*, 1999), it is also known that tumor cells retain WT p53. In this regard, functional inactivation of WT p53 by abnormal cytoplasmic sequestration is frequently observed in many tumor types (Moll *et al*, 1992, 1996; Schlamp *et al*, 1997). The RING finger protein Parc is considered to act as a cytoplasmic anchoring molecule of p53, but this clone does not have a p53 ubiquitination activity (Nikolaev *et al*, 2003). On the other hand, our present findings demonstrated that Synoviolin not only anchors p53 in the cytoplasm, but also ubiquitinates it, and thus differs from Parc (Figure 4). Moreover, Synoviolin diverges from other ligases for p53; each of the three ubiquitin ligases for p53 (MDM2, Pirh2 and Cop1) forms an autoregulatory negative feedback loop, resulting in lower p53 activity upon its expression, but these three ligases are target for the p53 transcriptional pathway (Dornan *et al*, 2004; Leng *et al*, 2003), whereas the expression of Synoviolin is not regulated by p53 (Figure 5F). Indeed, the *synoviolin* promoter region does not have a p53 target sequence, whereas it contains the ER stress responsive element (Tsuchimochi *et al*, 2005) and responds to the stress (Figure 5F). The reason for the multiple post-translational steps for p53 is the enormous importance of this molecule in maintaining cellular homeostasis. p53 is negatively regulated by various ubiquitin ligases, such as MDM2, MdmX, HAUSP, ARF, COP1, Pirh2 and ARF-BP1 (Brooks and Gu, 2006), and it is assumed that each molecule has its specific roles in p53 control. Among them, Synoviolin is also a unique regulator of p53 because of its independency from other ligases and transcriptional regulation by p53, ER localization and canonical function in ERAD.

In the present study, we demonstrated that Synoviolin participates in genotoxic stress-mediated p53 signaling, and its to participation in the ER stress-induced apoptosis is also well known (Bordallo *et al*, 1998; Kaneko *et al*, 2002; Kikkert *et al*, 2004; Yagishita *et al*, 2005). Therefore, Synoviolin seems to regulate two distinct apoptotic pathways and the ubiquitination of p53 by Synoviolin may be another target for crosstalk between them. Another linkage between ER stress and p53 pathway is also implicated by our finding that UPR markers are increased in cells with *synoviolin* knockdown (data not shown). Two reports described a crosstalk of p53- and ER stress- induced apoptosis pathways, that is, ER stress antagonizes p53-mediated apoptosis through the cytoplasmic localization of p53 due to phosphorylation by glycogen synthase kinase-3β (GSK-3β) (Qu *et al*, 2004), and p53 destabilization utilized the cooperative action of MDM2 and GSK-3β in ER-stressed cells (Pluquet *et al*, 2005). In this regard, it is important to note that UPR activation upon Synoviolin knockdown in RKO cells may be related to ER stress with impaired ERAD system. Since Synoviolin null cells show upregulation of p53, it is possible that the effect of p53 stabilization by Synoviolin knockdown exceeds the p53 destabilization effect of UPR induced by Synoviolin knockdown. This hypothesis may be supported by the finding that *synoviolin* siRNA treatment seemed to restore the expression of p53 at least in part, which was suppressed by ER stress (Figure 5F). The regulatory action of Synoviolin on p53 under ER stress is obviously more complex, because ER stress also induces Synoviolin expression. Further studies are necessary to determine the physiological regulatory role of Synoviolin in p53 expression under ER stress conditions.

The function of p53 in patients with RA is still controversial (Firestein *et al*, 1997; Reme *et al*, 1998; Inazuka *et al*, 2000; Muller-Ladner and Nishioka, 2000; Sun and Cheung, 2002). Mice lacking p53 do not develop spontaneous arthropathy but have severe collagen-induced arthritis (CIA) (Yamanishi *et al*, 2002; Simelyte *et al*, 2005). As we reported previously, overexpression of Synoviolin resulted in spontaneous arthropathy and its deficiency resulted in resistance to CIA in mice (Amano *et al*, 2003). Therefore, we assumed that the severity of arthritis could be determined by the Synoviolin–p53 control pathway and that the onset of spon-

taneous arthropathy may be caused by p53-independent pathway in these models. The influence of these relationships on arthritis is currently being examined in our laboratories, using *synoviolin* and p53 double null mutant mice. We hope that our research could uncover new pathogenic mechanisms of RA. Furthermore, since p53 is an important tumor suppressor gene, we believe that Synoviolin could be a useful therapeutic target for not only RA but also cancer based on its cytological and biochemical features, i.e., cytoplasmic localization and enzymatic activity (Hopkins and Groom, 2002).

In conclusion, we demonstrated that Synoviolin acts as an ERAD E3 ubiquitin ligase that controls cellular p53 and thus opens, a new concept for proliferative disorders such as RA and cancer.

Materials and methods

Plasmids

pcDNA3/Synoviolin WT or C307S-FLAG, pcDNA3/HA- and FLAG-p53, pcDNA3/MDM2 and pcDNA/HA-Ub plasmids have been described previously (Amano *et al*, 2003; Matsushita *et al*, 2005). Deletion of 53BD, MBP- and GST-fusions in Synoviolin deletion mutants was performed by PCR-based method in this study. To clone a cDNA encoding *Drosophila* homolog of human Synoviolin (dSyno), 2282 bp of CG1937 was cut out from EST GH11117 with *Eco*RI/*Xho*I, and subcloned into pUAST vector (Brand and Perrimon, 1993). The sequences of all plasmids generated by PCR were confirmed by ABI auto-sequencer.

Cells and transfections

RKO and HEK293 cells were cultured in Minimum Essential Medium (Sigma) and U2OS and Saos-2 in Dulbecco's modified Eagle's medium (Sigma). The sense sequences of siRNA oligonucleotides to *synoviolin* are (1) GGUGUUCUUUGGGCAACUG, (2) GCUGUGACAGAUGCCAUCA, (3) GGUUCUGCUGUACAUGGCC. Changes in p53 protein in RKO cells were determined by all these siRNAs. The sense sequence of siRNA oligonucleotides to *GFP* is GGCUACGUCCAGGAGCGC.

GST pull-down assay

GST-fusion proteins were expressed in *Escherichia coli* strain BL21 (Invitrogen) and purified by using glutathione-Sepharose beads (Amersham Biosciences). *In vitro*-translated ^{35}S-labeled p53 was pre-cleaned with 10 μg GST protein for 1 h at 4°C, followed by incubation with 10 μg of each GST-fusion protein in binding buffer (20 mM *N*-2-hydroxyethylpiperazine-*N*′-ethanesulfonic acid (HEPES), pH 7.9, 150 mM NaCl and 0.2% TritonX-100) for 1 h at 4°C. After washing, bound proteins were separated by SDS–PAGE and detected by BAS.

Immunoprecipitation assay

For co-immunoprecipitation assay between exogenous Synoviolin and exogenous p53, HEK293 cells were co-transfected with HA-p53 and pcDNA3-Synoviolin WT-FLAG, pcDNA3-SynoviolinΔ53BD-FLAG or pcDNA3-Synoviolin C307S-FLAG plasmids. Cell extracts were prepared with high-salt buffer (20 mM HEPES pH 7.2, 420 mM NaCl, 10% glycerol, 0.5% NP-40, 0.5 mM dithiothreitol (DTT), and 1 mM phenylmethylsulfonyl fluoride (PMSF)) and diluted at three-fold with 0.5 mM DTT and a protease inhibitor solution, followed by incubation with mouse IgG or anti-FLAG antibody. Precipitated proteins were detected by anti-HA or anti-FLAG antibodies.

To detect the interaction between endogenous Synoviolin and p53, HEK293 cells were lysed in 100 mM Tris–HCl, 80 mM NaCl, 1 mM EDTA, 5 mM EGTA, 5% glycerol, 2% (w/v) digitonin, 0.1% Brij 35, protease inhibitor cocktail and 20 μM of MG132. Immunoprecipitation was carried out in the presence or absence of SDS by using anti-p53 antibodies, anti-Synoviolin antibodies or control IgG. The immunoprecipitated samples were analyzed by western blot by using anti-p53 or anti-Synoviolin antibodies.

In vitro and in vivo ubiquitination assays

The *in vitro* ubiquitination assay was conducted as described previously (Amano *et al*, 2003). For the peptide inhibition assay, reaction solutions lacking no MBP-SynoviolinΔTM-6xHis and ATP were incubated with 53BD or control peptides (50, 100, and 200 μM) for 30 min at 4°C. Reactions were started by addition of MBP-SynoviolinΔTM-6xHis and ATP and incubating at 37°C.

For the *in vivo* ubiquitination assay, HEK293 cells were transfected with pcDNA3/HA-Ubiquitin, pcDNA3/FLAG-p53, and pcDNA3/Synoviolin WT, C307S or pcDNA3/MDM2. At 24 h post-transfection, cells were treated with MG132 (10 μM) for 1 h, then the cells were lysed in SDS containing buffer (50 mM Tris, pH 7.5, 0.5 mM EDTA, 1% SDS, and 1 mM DTT) and boiled for 5 min to denature the proteins. The denatured samples were diluted with immunoprecipitation buffer (50 mM Tris, pH 7.5, 2 mM EDTA, 150 mM NaCl, and 0.1% NP-40 and protease inhibitor cocktail) and the p53 protein was immunopurified by using anti-p53 antibody. Ubiquitinated p53 was detected by western blotting by using anti-HA antibody.

Immunostaining of fly wing discs

Fly wing discs were dissected in PBS, fixed in a buffer containing 50 mM Tris–HCl, pH 6.8, 1 mM EGTA, 1% Triton ×-100, 2 mM $MgSO_4$, 150 mM NaCl, and 2.2% formaldehyde for 15 min, and blocked using a blocking buffer (50 mM Tris–HCl, pH 6.8, 150 mM NaCl, 0.5% NP-40 and 5 mg/ml BSA). The fixed wing discs were incubated overnight at 4°C in a 1:200 dilution of anti-Dmp53 (d-200) antibody. After washing in a wash buffer (50 mM Tris–HCl, pH 6.8, 150 mM NaCl, 0.5% NP-40 and 1 mg/ml BSA), they were incubated for 3 h at 4°C in donkey anti-rabbit FITC at 1:200 dilution, washed with the wash buffer and then mounted in a mounting solution (50 mM Tris–HCl, pH 6.8, 30% glycerol, 150 mM NaCl, and 5 mg/ml phenylethylendiamine). The fluorescence intensity of each disc was quantified with Quantity One software (Bio-Rad Laboratories). Acridine orange staining was performed as reported previously (Brodsky *et al*, 2000).

Supplementary data

Supplementary data are available at *The EMBO Journal* Online (http://www.embojournal.org).

Acknowledgements

We are grateful to MR Montminy, G Verdine, R Nagata, H Shimizu, I Hishinuma, H Yokohama, H Kato, S Kitamura, K Yoshimatsu, Yuichiro ITAKURA OFFICE and ES Takagi, for advice and encouragement, and to H Takahashi, M Sato, S Otani, A Sugamiya, N Takagi, S Shinkawa, Y Nakagawa, Y Sato, M Yamanashi and members of Toshi's Laboratory for the excellent technical assistance. This study was supported in part by LocomoGene Inc., Eisai Co., Ltd, National Institute of Biomedical Innovation, the Japanese Ministry of Education, Culture, Sports, Science and Technology, the Japanese Ministry of Health, Labour and Welfare, the Kato Memorial Trust for Nanbyo Research, the Japan Medical Association, Nagao Memorial Fund, Kanae Foundation for Life & Socio-medical Science, Japan Research Foundation for Clinical Pharmacology, Kanagawa Nanbyo Foundation, Kanagawa Academy of Science and Technology Research Grants, Japan College of Rheumatology, the Nakajima Foundation, Japan Society for Promotion of Science, New Energy and Industrial Technology Development Organization, Mochida Pharmaceutical Co. Ltd, Kanto Bureau of Economy, Trade and Industry, and the Uehara Memorial Foundation. HF is supported by Japan Society for the Promotion of Science.

References

Amano T, Yamasaki S, Yagishita N, Tsuchimochi K, Shin H, Kawahara K, Aratani S, Fujita H, Zhang L, Ikeda R, Fujii R, Miura N, Komiya S, Nishioka K, Maruyama I, Fukamizu A, Nakajima T (2003) Synoviolin/Hrd1, an E3 ubiquitin ligase, as a novel pathogenic factor for arthropathy. *Genes Dev* **17**: 2436–2449

Bode AM, Dong Z (2004) Post-translational modification of p53 in tumorigenesis. *Nat Rev Cancer* **4**: 793–805

Bordallo J, Plemper RK, Finger A, Wolf DH (1998) Der3p/Hrd1p is required for endoplasmic reticulum-associated degradation of misfolded lumenal and integral membrane proteins. *Mol Biol Cell* **9:** 209–222

Brand AH, Perrimon N (1993) Targeted gene expression as a means of altering cell fates and generating dominant phenotypes. *Development* **118:** 401–415

Brodsky MH, Nordstrom W, Tsang G, Kwan E, Rubin GM, Abrams JM (2000) *Drosophila* p53 binds a damage response element at the reaper locus. *Cell* **101:** 103–113

Brooks CL, Gu W. (2006) p53 ubiquitination: Mdm2 and beyond. *Mol Cell* **21:** 307–315

Dornan D, Wertz I, Shimizu H, Arnott D, Frantz GD, Dowd P, O'Rourke K, Koeppen H, Dixit VM (2004) The ubiquitin ligase COP1 is a critical negative regulator of p53. *Nature* **429:** 86–92

Firestein GS, Echeverri F, Yeo M, Zvaifler NJ, Green DR (1997) Somatic mutations in the p53 tumor suppressor gene in rheumatoid arthritis synovium. *Proc Natl Acad Sci USA* **94:** 10895–10900

Fogh J, Wright WC, Loveless JD (1977) Absence of HeLa cell contamination in 169 cell lines derived from human tumors. *J Natl Cancer Inst* **58:** 209–214

Gottlieb E, Haffner R, King A, Asher G, Gruss P, Lonai P, Oren M (1997) Transgenic mouse model for studying the transcriptional activity of the p53 protein: age- and tissue-dependent changes in radiation-induced activation during embryogenesis. *EMBO J* **16:** 1381–1390

Harrison DA, Binari R, Nahreini TS, Gilman M, Perrimon N (1995) Activation of a *Drosophila* Janus kinase (JAK) causes hematopoietic neoplasia and developmental defects. *EMBO J* **14:** 2857–2865

Haupt Y, Maya R, Kazaz A, Oren M (1997) Mdm2 promotes the rapid degradation of p53. *Nature* **387:** 296–299

Hershko A, Ciechanover A (1998) The ubiquitin system. *Annu Rev Biochem* **67:** 425–479

Hollstein M, Hergenhahn M, Yang Q, Bartsch H, Wang ZQ, Hainaut P (1999) New approaches to understanding p53 gene tumor mutation spectra. *Mutat Res* **431:** 199–209

Hopkins AL, Groom CR (2002) The druggable genome. *Nat Rev Drug Discov* **1:** 727–730

Inazuka M, Tahira T, Horiuchi T, Harashima S, Sawabe T, Kondo M, Miyahara H, Hayashi K (2000) Analysis of p53 tumour suppressor gene somatic mutations in rheumatoid arthritis synovium. *Rheumatology* **39:** 262–266

Kaneko M, Ishiguro M, Niinuma Y, Uesugi M, Nomura Y (2002) Human HRD1 protects against ER stress-induced apoptosis through ER-associated degradation. *FEBS Lett* **532:** 147–152

Kastan MB, Onyekwere O, Sidransky D, Vogelstein B, Craig RW (1991) Participation of p53 protein in the cellular response to DNA damage. *Cancer Res* **51:** 6304–6311

Kikkert M, Doolman R, Dai M, Avner R, Hassink G, vanVoorden S, Thanedar S, Roitelman J, Chau V, Wiertz E (2004) Human HRD1 is an E3 ubiquitin ligase involved in degradation of proteins from the endoplasmic reticulum. *J Biol Chem* **279:** 3525–3534

Kubbutat MH, Jones SN, Vousden KH (1997) Regulation of p53 stability by Mdm2. *Nature* **387:** 299–303

Laney JD, Hochstrasser M (2003) Ubiquitin-dependent degradation of the yeast Mat(alpha)2 repressor enables a switch in developmental state. *Genes Dev* **17:** 2259–2270

Leng RP, Lin Y, Ma W, Wu H, Lemmers B, Chung S, Parant JM, Lozano G, Hakem R, Benchimol S (2003) Pirh2, a p53-induced ubiquitin-protein ligase, promotes p53 degradation. *Cell* **112:** 779–791

Matsushita N, Kitao H, Ishiai M, Nagashima N, Hirano S, Okawa K, Ohta T, Yu DS, McHugh PJ, Hickson ID, Venkitaraman AR, Kurumizaka H, Takata M (2005) A FancD2-Monoubiquitin Fusion Reveals Hidden Functions of Fanconi Anemia Core Complex in DNA Repair. *Mol Cell* **19:** 841–847

Meek DW (2004) The p53 response to DNA damage. *DNA Repair* **3:** 1049–1056

Moll UM, Ostermeyer AG, Haladay R, Winkfield B, Frazier M, Zambetti G (1996) Cytoplasmic sequestration of wild-type p53 protein impairs the G1 checkpoint after DNA damage. *Mol Cell Biol* **16:** 1126–1137

Moll UM, Riou G, Levine AJ (1992) Two distinct mechanisms alter p53 in breast cancer: mutation and nuclear exclusion. *Proc Natl Acad Sci USA* **89:** 7262–7266

Muller-Ladner U, Nishioka K (2000) p53 in rheumatoid arthritis: friend or foe? *Arthritis Res* **2:** 175–178

Nikolaev AY, Li M, Puskas N, Qin J, Gu W (2003) Parc: a cytoplasmic anchor for p53. *Cell* **112:** 29–40

Nishikawa S, Brodsky JL, Nakatsukasa K (2005) Roles of molecular chaperones in endoplasmic reticulum (ER) quality control and ER-associated degradation (ERAD). *J Biochem* **137:** 551–555

Ollmann M, Young LM, Di Como CJ, Karim F, Belvin M, Robertson S, Whittaker K, Demsky M, Fisher WW, Buchman A, Duyk G, Friedman L, Prives C, Kopczynski C (2000) *Drosophila* p53 is a structural and functional homolog of the tumor suppressor p53. *Cell* **101:** 91–101

Pickart CM (2001) Mechanisms underlying ubiquitination. *Annu Rev Biochem* **70:** 503–533

Pluquet O, Qu L, Baltzis D, Koromilas AE (2005) Endoplasmic reticulum stress accelerates p53 degradation by the cooperative actions of Hdm2 and Glycogen synthase kinase 3β. *Mol Cell Biol* **25:** 9392–9405

Ponten J, Saksela E (1967) Two established *in vitro* cell lines from human mesenchymal tumours. *Int J Cancer* **2:** 434–447

Qu L, Huang S, Baltzis D, Rivas-Estilla AM, Pluquet O, Hatzoglou M, Koumenis C, Taya Y, Yoshimura A, Koromilas AE (2004) Endoplasmic reticulum stress induces p53 cytoplasmic localization and prevents p53-dependent apoptosis by a pathway involving glycogen synthase kinase-3beta. *Genes Dev* **18:** 261–277

Reme T, Travaglio A, Gueydon E, Adla L, Jorgensen C, Sany J (1998) Mutations of the p53 tumour suppressor gene in erosive rheumatoid synovial tissue. *Clin Exp Immunol* **111:** 353–358

Schlamp CL, Poulsen GL, Nork TM, Nickells RW (1997) Nuclear exclusion of wild-type p53 in immortalized human retinoblastoma cells. *J Natl Cancer Inst* **89:** 1530–1536

Shaulsky G, Goldfinger N, Ben-Ze'ev A, Rotter V (1990) Nuclear accumulation of p53 protein is mediated by several nuclear localization signals and plays a role in tumorigenesis. *Mol Cell Biol* **10:** 6565–6577

Shearer AG, Hampton RY (2004) Structural control of endoplasmic reticulum-associated degradation: effect of chemical chaperones on 3-hydroxy-3-methylglutaryl-CoA reductase. *J Biol Chem* **279:** 188–196

Shearer AG, Hampton RY (2005) Lipid-mediated, reversible misfolding of a sterol-sensing domain protein. *EMBO J* **24:** 149–159

Simelyte E, Rosengren S, Boyle DL, Corr M, Green DR, Firestein GS (2005) Regulation of arthritis by p53: Critical role of adaptive immunity. *Arthritis Rheum* **52:** 1876–1884

Smith ML, Chen IT, Zhan Q, O'Connor PM, Fornace Jr AJ (1995) Involvement of the p53 tumor suppressor in repair of u.v.-type DNA damage. *Oncogene* **10:** 1053–1059

Sun Y, Cheung HS (2002) p53, proto-oncogene and rheumatoid arthritis. *Semin Arthritis Rheum* **31:** 299–310

Swanson R, Locher M, Hochstrasser M (2001) A conserved ubiquitin ligase of the nuclear envelope/endoplasmic reticulum that functions in both ER-associated and Matalpha2 repressor degradation. *Genes Dev* **15:** 2660–2674

Tsuchimochi K, Yagishita N, Yamasaki S, Amano T, Kato Y, Kawahara K, Aratani S, Fujita H, Ji F, Sugiura A, Izumi T, Sugamiya A, Maruyama I, Fukamizu A, Komiya S, Nishioka K, Nakajima T (2005) Identification of a crucial site for synoviolin expression. *Mol Cell Biol* **25:** 7344–7356

Vashist S, Ng DT (2004) Misfolded proteins are sorted by a sequential checkpoint mechanism of ER quality control. *J Cell Biol* **165:** 41–52

Vogelstein B, Lane D, Levine AJ (2000) Surfing the p53 network. *Nature* **408:** 307–310

Vousden KH, Lu X (2002) Live or let die: the cell's response to p53. *Nat Rev Cancer* **2:** 594–604

Wu J, Kaufman RJ (2006) From acute ER stress to physiological roles of the Unfolded Protein Response. *Cell Death Differ* **13:** 374–384

Yagishita N, Ohneda K, Amano T, Yamasaki S, Sugiura A, Tsuchimochi K, Shin H, Kawahara K, Ohneda O, Ohta T, Tanaka S, Yamamoto M, Maruyama I, Nishioka K, Fukamizu A, Nakajima T (2005) Essential role of synoviolin in embryogenesis. *J Biol Chem* **280:** 7909–7916

Yamanishi Y, Boyle DL, Pinkoski MJ, Mahboubi A, Lin T, Han Z, Zvaifler NJ, Green DR, Firestein GS (2002) Regulation of joint destruction and inflammation by p53 in collagen-induced arthritis. *Am J Pathol* **160:** 123–130

Effects of Cyclosporin A on the Activation of Natural Killer T Cells Induced by α-Galactosylceramide

Takashi Kajiwara,[1] Yukihiro Tomita,[1,6] Shinji Okano,[2] Toshiro Iwai,[1] Youichi Yasunami,[3] Yasunobu Yoshikai,[4] Kikuo Nomoto,[5] Hisataka Yasui,[1] and Ryuji Tominaga[1,6]

Background. Natural killer T (NKT) cells play crucial roles in preventing autoimmune diseases and inducing transplantation tolerance. We investigated whether cyclosporin A (CsA), which is generally used in clinical transplantation and autoimmune disease therapy, could modulate the NKT cell activation induced by α-galactosylceramide (α-GalCer) treatment.

Methods. C57BL/6 (B6) mice were given daily intraperitoneal injections of CsA (30 or 50 mg/kg) from day −1 and injected intravenously with α-GalCer (2 μg/mouse) on day 0. The kinetics of $NK1.1^+CD3^+$ or $NK1.1^+Thy1.2^+$ cells in the liver and spleen were analyzed by flow cytometry. Apoptosis of $NK1.1^+CD3^+$ cells, cytokine levels (interleukin [IL]-2, IL-4, IL-10 and interferon [IFN]-γ) in the recipient serum and changes in dendritic cell activation in the spleen were analyzed.

Results. In B6 mice treated with α-GalCer, $NK1.1^+CD3^+$ cells rapidly decreased in both the liver and spleen, and repopulated to their normal levels by day four, while $NK1.1^+Thy1.2^+$ cells rapidly decreased, expanded by day four and reduced to their normal level by day 15. When B6 mice were treated with α-GalCer plus 30 or 50 mg/kg CsA, $NK1.1^+CD3^+$ or $NK1.1^+Thy1.2^+$ cells were similarly decreased and then expanded via extensive proliferation by day seven or four, respectively. When B6 mice were treated with α-GalCer, substantial amounts of IL-2, IL-4 and IFN-γ were produced, and the surface markers of dendritic cells were upregulated. However, these cytokine productions and maturation of dendritic cells were profoundly suppressed after treatment with α-GalCer and CsA. Apoptosis of $NK1.1^+CD3^+$ cells was not affected in mice treated with α-GalCer or α-GalCer and CsA.

Conclusions. CsA suppresses α-GalCer-induced cytokine productions and dendritic cell maturation of mouse NKT cells but does not decrease $NK1.1^+CD3^+$ cells on day one. The modulation of NKT-mediated immunoregulatory functions by CsA requires careful consideration in clinical transplantation and autoimmune disease therapy.

Keywords: Natural killer T cells, Cyclosporin A, α-galactosylceramide.

(*Transplantation* 2007;83: 184–192)

Natural killer T (NKT) cells have been characterized as cells that coexpress the natural killer (NK) cell marker NK1.1 and the T-cell receptor (TCR) (*1–4*). Although their natural ligands have not been well characterized, NKT cells recognize and are strongly stimulated by a glycolipid antigen, α-galactosylceramide (α-GalCer), presented by the major histocompatibility complex (MHC) class I-like molecule CD1d (*5*). By using flow cytometry (FCM) and RNA extraction assays, initial studies have revealed that α-GalCer quickly activates NKT cells, which then become undetectable. This finding is correlated with increased apoptosis and increased expression of Fas and FasL by NKT cells (*6–8*). Another study reported a similar disappearance of NKT cells in vivo after stimulation with an anti-CD3 mAb or IL-12 (*9*). This demise of NKT cells after treatment with an anti-CD3 mAb or interleukin (IL)-12 was usually followed by repopulation within two to three days after the stimulation due to homeostatic proliferation in the bone marrow. On the other hand, more recent studies have suggested that receptor down-regulation is the primary cause of the NKT cell disappearance and reappearance following α-GalCer treatment (*10–12*).

After recognition of α-GalCer, NKT cells activate and rapidly secrete large amounts of both Th1 and Th2 cytokines, such as IL-4 and interferon (IFN)-γ (*5*). The activation of NKT cells has been considered to develop their immunoregulatory functions through Th1 and/or Th2 cytokines. NKT cells activated by α-GalCer have been shown to play important roles in preventing autoimmune diseases and enhancing anti-tumor cytotoxicity (*13–16*). In transplant immunity, NKT cells play vital roles in the induction of not only allograft tolerance but also xenograft tolerance, although the precise mechanisms for these effects have not yet been clarified (*17, 18*).

Cyclosporin A (CsA) is a popular immunosuppressive drug that is widely used in organ transplantation and autoimmune disease therapy. In mice, a middle dose (30 mg/kg) of CsA suppresses IL-2 production by $CD4^+$ helper T cells, whereas a high dose (75 mg/kg) suppresses that by both $CD4^+$ and $CD8^+$ helper T cells (*19*). Paradoxically, however, CsA can cause autoimmune diseases (*20, 21*) and a graft-versus-host (GVH)-like syndrome in syngeneic bone marrow transplantation (*22, 23*), and interfered with the induction of allograft tolerance in rodents (*24*). Because NKT cells play

This study was supported by a grant-in-aid (to Yukihiro Tomita) for Scientific Research from the Ministry of Health and Welfare, Japan.

[1] Department of Cardiovascular Surgery, Faculty of Medicine, Kyushu University, Fukuoka, Japan.
[2] Department of Pathology I, Faculty of Medicine, Kyushu University, Fukuoka, Japan.
[3] Department of Surgery I, Fukuoka University School of Medicine, Fukuoka, Japan.
[4] Department of Infection Control, Medical Institute of Bioregulation, Kyushu University, Fukuoka, Japan.
[5] Department of Immunology, Medical Institute of Bioregulation, Kyushu University, Fukuoka, Japan.
[6] Address correspondence to: Yukihiro Tomita, M.D., Ph.D., Department of Cardiovascular Surgery, Faculty of Medicine, Kyushu University, 3-1-1 Maidashi, Higashi-ku, Fukuoka 812-8582, Japan.
E-mail: tomita@heart.med.kyushu-u.ac.jp

Received 4 October 2005. Revision requested 3 October 2006.
Accepted 5 October 2006.

ISSN 0041-1337/07/8302-184
DOI: 10.1097/01.tp.0000250573.50046.89

essential roles in the maintenance of tolerance and prevention of autoimmune diseases, breakdown of the transplantation tolerance or autoimmune disease prevention induced by CsA may be caused via the suppression of NKT cell functions.

Therefore, in the present study, we investigated whether middle and high doses of CsA (30 and 50 mg/kg, respectively) could modulate the activation of NKT cells following treatment with α-GalCer on day 0. After treatment with α-GalCer and CsA, a similar rapid disappearance of $NK1.1^+CD3^+$ cells was observed on day one, but these cells subsequently increased to a higher level than that after treatment with α-GalCer alone. Cytokine productions were completely suppressed and $CD11c^+$ dendritic cells did not become mature after treatment with α-GalCer and CsA. These results indicate that CsA could completely suppress the cytokine productions by NKT cells, but did not down-regulate their surface markers. Therefore, the results of the present study suggest that suppression of the immunoregulatory functions of NKT cells by CsA may be one of the causes of autoimmune disease development and interfere with tolerance induction.

MATERIALS AND METHODS

Animals

Inbred female mice of the C57BL/6 SnSlc (B6; $H\text{-}2^b$) strain were obtained from Japan SLC Inc. (Hamamatsu, Shizuoka, Japan), and used at 8–16 weeks of age. All animals received humane care in compliance with both the Guidelines for Animal Experiments of Kyushu University and the Law (No. 105) and Notification (No. 6) of the Japanese government.

Reagents

α-GalCer (KRN7000) was kindly provided by Kirin Brewery (Takasaki, Japan), dissolved in 0.5% polysorbate 20 at a concentration of 200 μg/ml and then further diluted with 0.9% NaCl. CsA (Novartis Pharmaceuticals, Basel, Switzerland) was dissolved in 0.9% NaCl at a concentration of 2 mg/ml.

In Vivo Treatments

Mice were injected intravenously (i.v.) with 2 μg of α-GalCer. As a control, mice were injected with an equivalent amount of vehicle, namely 0.5% polysorbate 20 and 0.9% NaCl. From one day before the α-GalCer treatment, mice received daily intraperitoneal (i.p.) injections of CsA (30 or 50 mg/kg). The day of the α-GalCer injection is referred to as day 0 throughout this report.

Cell Preparation

Mice were sacrificed by decapitation, and cell suspensions were prepared from the liver and spleen. The liver was disrupted in Roswell Park Memorial Institute (RPMI) 1640 medium (Gibco, Grand Island, NY) supplemented with 10% fetal calf serum (FCS) by pressing the liver fragments between two glass slides, then washed, resuspended in 40% isotonic Percoll solution (Amersham Biosciences, Piscataway, NJ) and overlaid on 67.5% isotonic Percoll solution. Following centrifugation at 3000 rpm for 30 min at room temperature, liver mononuclear cells (LMNC) were isolated from the interface, washed twice with Hanks balanced salt solution (HBSS) containing 2% FCS and then resuspended in the same solution. The spleen was disrupted in RPMI 1640 medium in the same manner as the liver, and then washed with HBSS containing 2% FCS. The spleen cell (SC) suspensions obtained were filtered through cotton gauze and washed twice with HBSS containing 2% FCS. Viable nucleated cells were counted and usually adjusted to 1×10^7 cells/mL.

Thymectomy

Recipients were anesthetized by an i.p. administration of 50 mg/kg phenobarbital (Nembutal; Shionogi, Osaka, Japan). After a partial sternotomy, a thymectomy was performed via an en bloc excision using two forceps (*25*). The absence of thymic tissue was always confirmed when the thymectomized animals were sacrificed, and animals showing the presence of residual thymic tissue were excluded from the analysis.

Flow Cytometry

The surface phenotypes of the LMNC and SC were identified by two-color FCM. Cells were incubated with phycoerythrin (PE)-conjugated anti-NK1.1 or anti-CD5 (BD PharMingen, San Diego, CA), biotin-conjugated anti-CD3e or anti-NK1.1 (BD PharMingen) monoclonal antibodies (mAbs) and fluorescein isothiocyanate (FITC)-conjugated anti-Thy1.2 (BD PharMingen) for 60 min at 4°C and then washed twice with HBSS containing 2% FCS. Biotin-conjugated reagents were developed with FITC- or allophycocyanin (APC)-conjugated streptavidin (SA; BD PharMingen).

To detect the NKT cells undergoing apoptosis, three-color FCM was used. LMNC were isolated at three hr after the α-GalCer injection. The cells were stained with PE-conjugated anti-NK1.1 (BD PharMingen) and biotin-conjugated anti-CD3e (BD PharMingen) mAbs. Biotin-conjugated reagents were developed with APC-SA (BD PharMingen). Cells were washed twice in annexin V binding buffer (BD PharMingen) before labeling with FITC-conjugated annexin V (BD PharMingen) for 30 min at room temperature in the dark.

To analyze the maturation of dendritic cells (DC), SC were isolated at 24 hr after the α-GalCer injection. The cells were stained with FITC-conjugated anti-CD11c (BD PharMingen) and PE-conjugated anti-$I\text{-}A^b$ (BD PharMingen), anti-CD40 (BD PharMingen), anti-CD80 (BD PharMingen) or anti-CD86 (BD PharMingen) mAbs for 30 min at 4°C. To block nonspecific FcγR receptor binding of the labeled antibodies, 10 μL of an undiluted culture supernatant containing 2.4G2 (a rat antimouse FcγR mAb) was added to the first incubation, and then washed. All data were analyzed with a FACSCalibur (Becton Dickinson, Sunnyvale, CA). Dead cells were excluded by gating out low forward scatter and high propidium iodide-retaining cells.

Cytokine Secretion Following In Vivo α-GalCer Treatment

Mice were injected with either α-GalCer or vehicle alone and then bled after 2 or 18 hr. The cytokine levels (IL-2, IL-4, IL10 and IFN-γ) in the serum were determined using a standard sandwich enzyme-linked immunosorbent assay (ELISA) (BioSource International Inc., Camarillo, CA).

Statistics

The statistical significance of the data was determined using Students *t* test. A *P* value of less than 0.05 was considered to be statistically significant.

RESULTS

Kinetics of the Percentages of NK1.1$^+$CD3$^+$ Cells in the Liver and Spleen of Recipient Mice Treated with α-GalCer and CsA

When α-GalCer is administered to B6 mice, a rapid reduction followed by restoration has been shown for NK1.1$^+$CD3$^+$ cells among the LMNC and SC (*6, 26*). Here, we examined the effects of CsA on the kinetics of NK1.1$^+$CD3$^+$ cells induced by α-GalCer. A middle or high dose of CsA (30 or 50 mg/kg, respectively) was injected i.p. daily from one day before the α-GalCer treatment. As shown in Figure 1A, the percentage of NK1.1$^+$CD3$^+$ cells in the LMNC rapidly decreased to less than 2% on day one, was restored to around 8% by day four and then remained constant until day 15 in mice treated with α-GalCer. In the LMNC of mice treated with α-GalCer plus 30 mg/kg CsA, the NK1.1$^+$CD3$^+$ cells were reduced to less than 2% on day one, restored to the normal level by day seven and then reduced to about 13% by day 15. In the LMNC of mice treated with α-GalCer plus 50 mg/kg CsA, the NK1.1$^+$CD3$^+$ cells were similarly reduced to less than 2% on day one, restored to above the normal level by day seven and then reduced to the normal level by day 15. Similar results were observed for the SC of mice treated with α-GalCer plus 30 or 50 mg/kg CsA, and representative data are shown in Figure 1A. We analyzed the early response of NKT cells after treatment with α-GalCer or α-GalCer and CsA by using other T-cell markers such as CD5 or Thy1.2. The kinetics of the NK1.1$^+$CD5$^+$ cells after treatment with α-GalCer or α-GalCer and CsA were same as those observed for the NK1.1$^+$CD3$^+$ cells (data not shown). The kinetics of the NK1.1$^+$Thy1.2$^+$ cells in the liver and spleen of recipient mice treated with α-GalCer and CsA are shown in Figure 1B. In the liver of mice treated with α-GalCer alone, NK1.1$^+$Thy1.2$^+$ cells rapidly decreased on day one and repopulated by day four. In the liver of mice treated with α-GalCer plus 30 or 50 mg/kg CsA, NK1.1$^+$Thy1.2$^+$ cells also decreased on day one and then gradually increased by days 7 to 15. In the spleen of mice treated with α-GalCer alone or α-GalCer plus 30 or 50 mg/kg CsA, NK1.1$^+$Thy1.2$^+$ cells rapidly decreased on day one, increased to above the normal level by days four and seven and then returned to the normal level on day 15.

Kinetics of the Numbers of NK1.1$^+$CD3$^+$ Cells among the LMNC and SC of Mice Injected with α-GalCer and CsA

We further examined the numbers of total cells and NK1.1$^+$CD3$^+$ cells in the liver after treatment with α-GalCer and CsA. The LMNC counts did not change significantly on day one, increased by day four and then decreased to the normal level by day 15 in mice treated with α-GalCer alone or α-GalCer plus 30 or 50 mg/kg CsA (Fig. 2a). The LMNC dramatically increased in mice treated with α-GalCer alone (~fourfold) and α-GalCer plus 30 or 50 mg/kg CsA (~six- to eight-fold) on day four. These expansions of the LMNC number on day four showed significant differences between mice treated with α-GalCer alone and those treated with α-GalCer plus 30 or 50 mg/kg CsA. Similar results were observed for the changes in the SC counts, although the LMNC were more extensively increased than the SC.

In the liver of mice treated with α-GalCer alone, the NK1.1$^+$CD3$^+$ cell counts rapidly decreased on day one, were restored to the normal level by day four and then gradually decreased by day 15 (Fig. 2b). On the other hand, the NK1.1$^+$CD3$^+$ cell counts in the liver of mice treated with α-GalCer plus 30 or 50 mg/kg CsA showed similar decreases on day one, then increased to above the normal level by day four, further increased on day seven (~fourfold) and gradually decreased by day 15. There were significant differences in the NK1.1$^+$CD3$^+$ cell numbers between mice treated with α-GalCer alone and those treated with α-GalCer plus 30 or 50 mg/kg CsA on day seven. Similar results were observed for the changes in the spleen NKT cell counts. As shown in Figure 1A, NK1.1$^+$CD3$^+$ cells in mice treated with α-GalCer plus 30 or 50 mg/kg CsA were still decreased on day four and repopulated by day seven. Therefore, the number of NK1.1$^+$CD3$^+$ cells showed the largest increase on day seven, while the total number of LMNC showed the largest increase on day four. NK1.1$^+$Thy1.2$^+$ cells in the liver and spleen of mice treated with α-GalCer alone or α-GalCer plus 30 or 50 mg/kg CsA showed rapid decreases on day one and expansion on day four (Fig. 2c).

Effects of Thymectomy on the Kinetics of the NK1.1$^+$CD3$^+$ Cell Counts After Treatment with α-GalCer and CsA

Many studies have suggested that the thymus is involved in the normal development of NKT cells. Therefore, we investigated whether the thymus was involved in the repopulation of NK1.1$^+$CD3$^+$ cells after treatment with α-GalCer and CsA by using thymectomized B6 mice. In thymectomized mice treated with α-GalCer alone or α-GalCer plus 30 or 50 mg/kg CsA, the percentage of NK1.1$^+$CD3$^+$ cells in the LMNC rapidly decreased on day one, remained the same on day four and was then restored to above the normal level by day seven. Therefore, the NK1.1$^+$CD3$^+$ cells in thymectomized mice showed the same kinetics as those in nonthymectomized mice (Fig. 3).

In Vivo Cytokine Responses at 2 or 18 Hours After Injection of α-GalCer and CsA

To further examine the effects of CsA on the α-GalCer-induced activation of NKT cells, the productions of Th1 (IL-2 and γ-IFN) and Th2 (IL-4 and IL-10) cytokines were measured. At 2 and 18 hr after the administration of α-GalCer, serum was collected from the mice and the level of each cytokine was determined using a standard sandwich ELISA. Consistent with previous studies (*7, 13, 14*), α-GalCer treatment induced the productions of IL-2, IL-4 and γ-IFN (Fig. 4). However, these cytokine productions were almost abrogated in the serum of mice treated with α-GalCer plus 30 or 50 mg/kg CsA.

Maturation of DC After Intravenous Injection of α-GalCer and CsA

A recent report (*27*) demonstrated that α-GalCer treatment induces the maturation of splenic CD11c$^+$ DC, as indi-

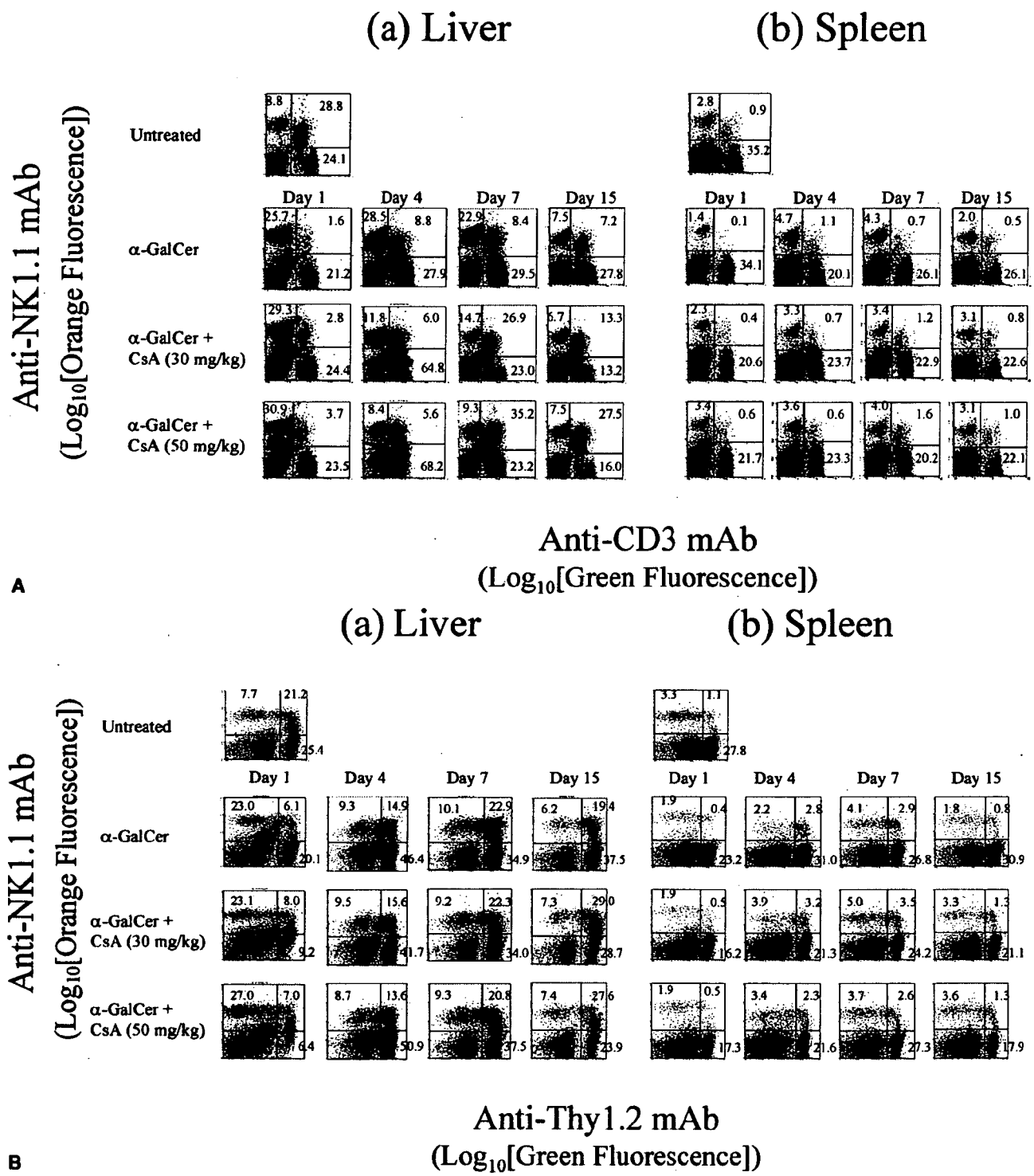

FIGURE 1. Phenotypic characterization of NK1.1$^+$ CD3$^+$ cells by two-color immunofluorescence. B6 mice were injected with α-GalCer on day 0 and CsA (30 or 50 mg/kg) daily from one day before the α-GalCer treatment. The cells were labeled with PE-conjugated anti-NK1.1 and FITC-conjugated anti-CD3 mAbs (A) or PE-conjugated anti-NK1.1 and FITC-conjugated anti-Thy1.2 mAbs (B). Liver mononuclear cells (a) and spleen cells (b) were isolated after the indicated times and analyzed by flow cytometry. The numbers indicate the percentage of cells in the quadrant relative to the total cell population. The experiment shown is representative of four independent experiments.

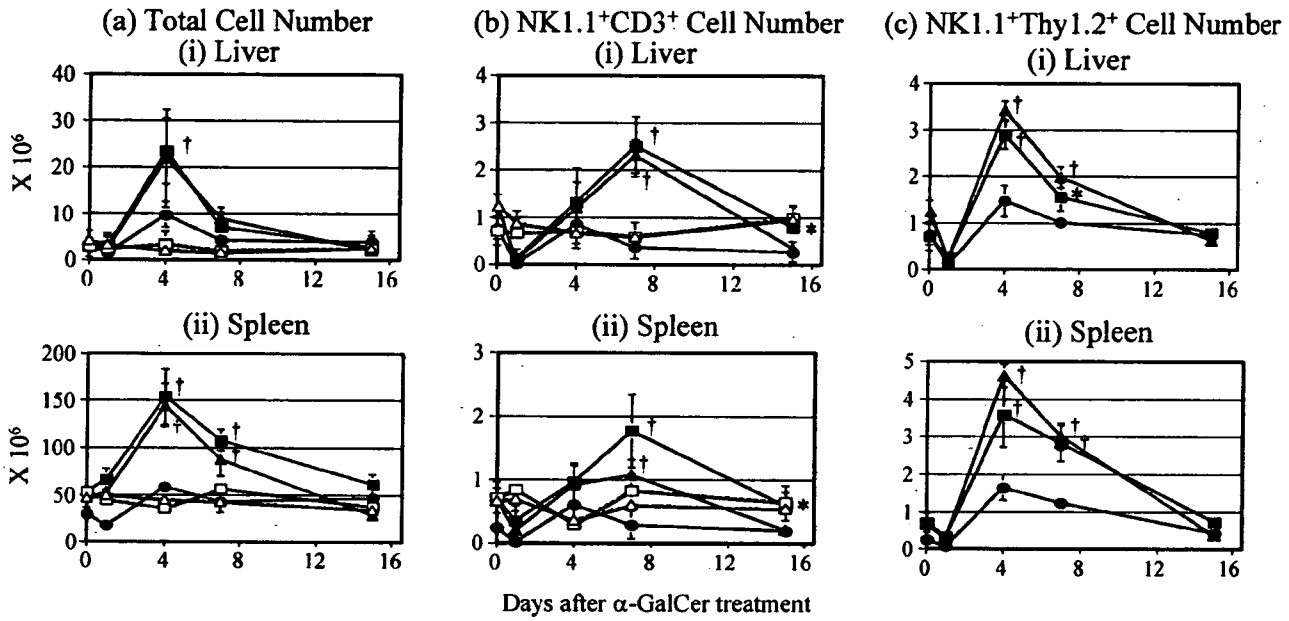

FIGURE 2. Influence of CsA on the induction of cell proliferation after α-GalCer treatment. Cells were labeled with PE-conjugated anti-NK1.1 and FITC-conjugated anti-CD3 mAbs or PE-conjugated anti-NK1.1 and FITC-conjugated anti-Thy1.2 mAbs. The kinetics of the total cell numbers (a), $NK1.1^+CD3^+$ cells (b) and $NK1.1^+Thy1.2^+$ cells (c) in the liver mononuclear cells and spleen cells of B6 mice treated with α-GalCer and CsA are shown. B6 mice were injected with α-GalCer on day 0 and CsA (30 or 50 mg/kg) daily from one day before the α-GalCer treatment. Liver and spleen cells were obtained from B6 mice treated with α-GalCer alone (● n=4), α-GalCer plus 30 mg/kg CsA (▲ n=4), α-GalCer plus 50 mg/kg CsA (■ n=4), 30 mg/kg CsA alone (Δ n=4) or 50 mg/kg CsA alone (□ n=4). Vertical bars represent the SD. *$P<0.05$, †$P<0.01$ vs. mice treated with α-GalCer alone.

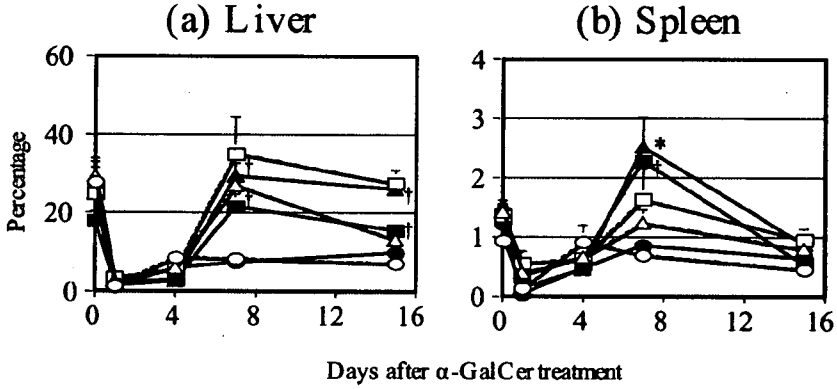

FIGURE 3. Kinetics of $NK1.1^+CD3^+$ cells in thymectomized mice treated with α-GalCer and CsA. The kinetics of the mean percentages of $NK1.1^+CD3^+$ cells in the liver mononuclear cells (a) and spleen cells (b) of thymectomized B6 mice treated with α-GalCer and CsA are shown. Cells were labeled with PE-conjugated anti-NK1.1 and FITC-conjugated anti-CD3 mAbs. B6 mice were thymectomized at four weeks before the α-GalCer treatment. The thymectomized mice were i.v. injected with α-GalCer (2 μg) on day 0 and i.p. injected with CsA (30 or 50 mg/kg) daily from one day before the α-GalCer treatment. Liver and spleen cells were obtained from non-thymectomized B6 mice treated with α-GalCer alone (○ n=4), α-GalCer plus 30 mg/kg CsA (Δ; n=4) or α-GalCer plus 50 mg/kg CsA (□ n=4), and from thymectomized B6 mice treated with α-GalCer alone (● n=4), α-GalCer plus 30 mg/kg CsA (▲ n=4) or α-GalCer plus 50 mg/kg CsA (■ n=4). Vertical bars represent the SD *$P<0.05$, †$P<0.01$ vs. mice treated with α-GalCer alone.

cated by the up-regulation of $I\text{-}A^b$, CD40, CD80 and CD86. At 24 hours after α-GalCer treatment, SC were stained with FITC-conjugated anti-CD11c and PE-conjugated anti-$I\text{-}A^b$, CD40, CD80 or CD86 mAbs, and the $CD11c^+$ cells were analyzed. As shown in Table 1, the expressions of $I\text{-}A^b$, CD40, CD80, and CD86 were clearly augmented in the $CD11c^+$ SC of mice treated with α-GalCer alone compared with those of untreated mice. The increases in the CD40, CD80, and CD86 expressions were lower in the $CD11c^+$ SC of mice treated with α-GalCer plus 30 or 50 mg/kg CsA than in those of mice treated with α-GalCer alone. On the other hand, the expression of $I\text{-}A^b$ was not augmented in the $CD11c^+$ SC of mice

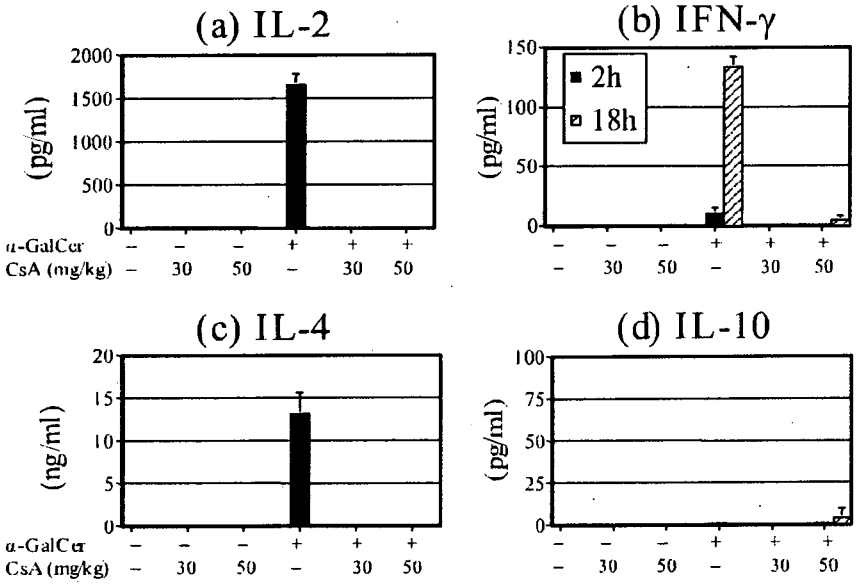

FIGURE 4. Production of Th1 and Th2 cytokines in B6 mice at 2 and 18 hr after α-GalCer treatment. B6 mice were injected with CsA (30 or 50 mg/kg) one day before the α-GalCer treatment. The serum levels of IL-2 (a), IFN-γ (b), IL-4 (c), and IL-10 (d) at 2 and 18 hr after injection of α-GalCer or vehicle were determined by ELISA. The data shown are the mean±SD of three mice for each group.

TABLE 1. Maturation of surface markers on splenic dendritic cells at 24 hours after treatment with α-GalCer and CsA

Group	Treatment[a]		No. of mice	Median fluorescence intensity (mean values±SD)			
	α-GalCer (2 μg)	CsA (mg/kg)		I-A[b]	CD40	CD80	CD86
1	–	—	4	1174.6±74.2	46.8±6.2	51.5±2.5	40.2±5.5
2	–	30	4	848.1±82.2	37.9±4.7	49.0±5.1	38.4±3.2
3	–	50	4	633.8±83.7	36.7±3.6	40.7±5.4	37.7±4.6
4	+	—	4	2714.4±51.8[b]	151.2±9.8[b]	186.8±17.5[b]	413.6±32.6[b]
5	+	30	4	865.4±310.9[c]	66.5±16.6[c,e]	59.0±6.5[c]	72.2±16.7[c,e]
6	+	50	4	681.8±91.6[c]	67.1±6.6[d,e]	53.1±4.1[d,e]	71.7±18.5[d,e]

[a] Mice received CsA on days −1 and 0 and were injected with α-GalCer on day 0.
[b] $P<0.01$ vs. Group 1.
[c] $P<0.05$ vs. Group 2.
[d] $P<0.05$ vs. Group 3.
[e] $P<0.01$ vs. Group 4.

treated with α-GalCer plus 30 or 50 mg/kg CsA compared with those of mice treated with CsA alone. However, the augmentations of all these molecules were suppressed in the $CD11c^+$ SC of mice treated with α-GalCer plus 30 or 50 mg/kg CsA compared with those of mice treated with α-GalCer alone.

α-GalCer-Induced Apoptosis of $NK1.1^+CD3^+$ Cells After Treatment with α-GalCer and CsA

Depletion of $NK1.1^+CD3^+$ cells among the LMNC and SC is already observed at three hours after the administration of α-GalCer, and most of the $NK1.1^+CD3^+$ cells become undetectable at 24 hours after the α-GalCer injection. Previous reports have shown that liver $NK1.1^+CD3^+$ cells from α-GalCer-treated mice exhibit a significant increase in annexin V binding at three hours after the injection compared to those from control mice (*6, 7*). This observation indicates that the rapid depletion of $NK1.1^+CD3^+$ cells after α-GalCer treatment is primarily due to apoptotic cell death. However, a recent study showed no significant increase in annexin V binding in liver $NK1.1^+CD3^+$ cells in α-GalCer-treated mice (*11*). Therefore, we tested whether liver NKT cells exhibited an increase in annexin V binding at three hours after the injection of α-GalCer and CsA (Table 2). The median fluorescence intensity (MFI) and percentage of annexin V-positive $NK1.1^+CD3^+$ cells in the LMNC of mice treated with CsA alone did not differ significantly from those in untreated mice. Moreover, the MFI and percentage of annexin V-positive $NK1.1^+CD3^+$ cells in the LMNC of mice treated with α-GalCer alone did not increase significantly compared with those in untreated mice. Similarly, there were no significant changes in the MFI values and percentages of annexin V-positive $NK1.1^+CD3^+$ cells of mice treated with α-GalCer plus 30 or 50 mg/kg CsA.

DISCUSSION

NKT cells have been characterized as cells that express an invariant Vα14 TCR together with the NK cell marker NK1.1. To date, a number of studies have reported on the unique characteristics and physiological functions of NKT cells (*28*). NKT cells recognize a glycolipid antigen, α-GalCer,